

Flying the TRMM Satellite in a GCM

Xin Lin, Laura D. Fowler, and David A. Randall

Department of Atmospheric Science

Colorado State University

Fort Collins, CO 80523

March 5, 2001

Submitted to *the Journal of Geophysical Research*

Corresponding author's address:

Dr. Xin Lin

Department of Atmospheric Science

Colorado State University

Fort Collins, CO 80523

Email: lin@atmos.colostate.edu

Abstract

By incorporating the Tropical Rainfall Measurement Mission (TRMM) satellite orbital information into the Colorado State University General Circulation Model (CSU GCM), we are able to “fly” a satellite in the GCM, and sample the simulated atmosphere in the same way as the TRMM sensors sample the real atmosphere. The TRMM-sampled statistics for precipitation and radiative fluxes at annual, intraseasonal, monthly-mean and seasonal-mean diurnal time scales are evaluated by comparing the satellite-sampled against fully-sampled simulated atmospheres.

The sampling rates of the TRMM sensors are significantly affected by the sensors' swath widths. The TRMM Microwave Imager (TMI) and the Visible Infrared Scanner (VIRS) sample each $2.25^{\circ} \times 2.25^{\circ}$ grid box in the Tropics and subtropics about once per day, but at a different local time every day, while the Precipitation Radar (PR) and the Clouds and the Earth's Radiant Energy System (CERES) sensor visit each grid box about once every three days and twice per day, respectively. Besides inadequate samplings resulting from sensors' swath widths, there is a large, systematic diurnal undersampling associated with TRMM's orbital geometry for grid boxes away from the Equator. When only one month of TRMM data are used, this diurnal undersampling can lead to more daytime samples relative to nighttime samples in one hemisphere, and more nighttime samples relative to daytime samples in the other hemisphere. The resulting sampling biases ($3-6 \text{ W m}^{-2}$) are very pronounced in outgoing longwave radiation (OLR) over the subtropical land masses.

The sampling errors in OLR monthly- and seasonal-means are less than 8 W m^{-2} (5%) for each $2.25^{\circ} \times 2.25^{\circ}$ grid box. The OLR monthly- and seasonal-means are not sensitive to diurnal undersamplings associated with the TRMM orbits and sensors' swath widths. However, this is not the case for total precipitation. Diurnal undersampling could produce errors as large as 20% in the Tropics and 40% in the subtropics, for the zonally averaged monthly-mean rain rates.

The TRMM orbits sample each $2.25^{\circ} \times 2.25^{\circ}$ grid box in the Tropics and subtropics 1-6 times for each hour of the day within a single season. The seasonal-mean diurnal cycles of precipitation and OLR are not well sampled for any one grid box. By either accumulating the satellite data for a long enough period, or averaging the data over a large area with a relatively uniform diurnal signal, the diurnal cycles of precipitation and OLR can be satisfactorily sampled.

The effects TRMM sampling errors on the inferred tropical-mean hydrologic cycle and radia-

tive fluxes are also evaluated. There are strong spurious oscillations associated with TRMM's orbital geometry, with periods of 23 days and 3-4 months, in tropical-mean daily and monthly precipitation. While the relative fluctuations of the sampled-OLR are negligible, the relative fluctuations of the sampled precipitation have magnitudes similar to those of the observed climate variability. Caution must therefore be used when applying TRMM observations of tropical-mean precipitation to interpret climate variations at intraseasonal and interannual scales.

1. Introduction

Satellite data have been widely utilized in studies of global climate, to obtain global distributions of precipitation, top-of-the-atmosphere radiative fluxes, temperature and winds, as well as clouds and aerosols (e.g., Kidder and Vonder Haar 1995). Studies based on satellite data have greatly improved our understanding of climate variability and the hydrologic cycle, and have helped to improve physical parameterizations used in climate and numerical weather prediction models.

One major advantage of satellite data is that they can, over extended periods, cover areas where in-situ observations are not available, especially over the open oceans. However, this is accomplished at the expense of a reduced sampling rate compared to typical surface observations over land. Unlike in-situ observations, which can be made regularly (typically a few times per day at regular time intervals), most non-geostationary satellites circling the globe visit a specific location only once or twice a day or even less, depending on their orbital characteristics and sensor swath widths. Besides algorithm-related retrieval errors, monthly-mean and seasonal-mean meteorological fields obtained with satellite data may have large uncertainties due to inadequate sampling, especially on short time scales (e.g., Salby 1988; Bell et al. 1990; Zeng and Levy 1995; Salby and Callaghan 1997; Engelen et al. 2000; Fowler et al. 2000), and so may not faithfully capture what occurs in nature. This sampling uncertainty has always been an important issue in satellite mission planning (e.g., North 1988; Shin and North 1988; Bell et al. 1990; Bell and Kundo 1996; Fowler et al. 2000; Bell and Kundo 2000), and must be examined before we can efficiently use satellite data to investigate natural variability and to evaluate climate simulations.

The sampling error is a complicated function of the orbital geometry and statistical properties of the measured fields (e.g., Bell et al. 1990; Li et al. 1996). As a feasibility study for the Tropical Rainfall Measurement Mission (TRMM; Simpson et al. 1988; Simpson et al. 1996), North (1988) reviewed sampling studies that had been conducted using both real data from the GARP Atlantic Tropical Experiment (GATE) and artificially generated data from stochastic models. Assuming that the instruments made perfect measurements, North (1988) estimated sampling errors of 10% in monthly rain rate for TRMM-sized boxes (600 by 600 km) and for the low-altitude, low-inclination orbit. Shin and North (1988) further examined the TRMM sampling charac-

teristics by accounting for varying return intervals and partial sampling of the averaging area on a given visit. Their study suggested that the sampling error would be about 8-12% for monthly mean rain rates over a grid box of $5^{\circ} \times 5^{\circ}$. Similar conclusions were drawn by Bell et al. (1990) using a stochastic model. Bell and Reid (1993), Soman et al. (1995), and Li et al. (1996) also examined the diurnal cycle statistics of rainfall by simulating a satellite flying over the GATE and Darwin areas, respectively.

The earlier satellite sampling studies (e.g., Leith 1973; McConnell and North 1987; Bell 1987; North 1988; Bell et al. 1990; Bell and Reid 1993; Soman et al. 1995; Bell and Kundu 1996; Li et al. 1996; Huffman 1997) have provided many valuable insights into monthly-mean and diurnal rainfall statistics. However, there are limitations to these studies. As pointed by North (1988), Bell et al. (1990), and Li et al. (1996), most satellite precipitation statistics were derived for the GATE and Darwin areas where surface observations were available, and it is uncertain if the same statistics are applicable to other regions of the globe. In addition, most surface observational records used in satellite sampling studies are short (e.g., there are only 18 days in GATE Phase I), and a simulated satellite may not obtain statistically-meaningful samples within that period. Furthermore, different sensors aboard a satellite may have different swath widths, and the measured climate variables may have significantly different sampling statistics. Besides precipitation amount statistics, similar studies of other important climate variables such as precipitation frequency and intensity, radiative fluxes, etc., have not been examined, due in part to the lack of suitable observations.

The TRMM satellite was launched in November 1997 to determine the temporal and spatial distributions of precipitation and radiative fluxes in the tropics and subtropics. TRMM's orbit is circular, with an inclination of 35° to the Equator. The satellite visits low latitudes about once per day, but at a different local time every day. Therefore, unlike data collected from polar-orbiting satellites, TRMM data can be used to investigate tropical climate variability at both monthly-mean and shorter time scales when accumulated for a long enough period.

Ideally, we would like to have long-term **real** observations on the global scale to evaluate the satellite sampling statistics at monthly-mean and composite diurnal time scales. This is not possible in the real world. Model-dependent reanalyses are good candidates for providing "truth"

observations, but most current reanalyses provide only 6-hourly data. In this study, we use a general circulation model (GCM) to generate simulated data by assuming that the GCM can realistically simulate the atmosphere at annual, seasonal, monthly, and diurnal time scales. Figure 1 is a schematic showing how we can investigate satellite sampling issue with the help of a GCM. X stands for an unknown climate variable (e.g., precipitation amount) that we would like to observe perfectly but cannot. The only data we can obtain are sampled or "observed" X , X_{obs} . The deviation ϵ is $X_{\text{obs}} - X$, and the sampling error σ , as defined in Bell et al (1990), is $\{(X_{\text{obs}} - X)^2\}^{0.5}$. Before we can evaluate climate simulations using such sampled observations, we need to understand σ and ϵ . However, since X is what we really want to obtain, we are not able to compare directly the sampled variable and the real variable. A GCM can continuously simulate the same climate variable, and therefore the simulated climate variable can be considered "known". If we fly a virtual satellite in the GCM, using the same orbit as the real satellite, we can compare the GCM-simulated field with the sampled GCM-simulated field at various time scales. The sampling errors of the satellite observations can then be inferred from such comparisons.

In this study, we have combined the Colorado State University (CSU) GCM and the TRMM orbital data to explore the sampling statistics of the sensors onboard the TRMM satellite. Section 2 briefly discusses the TRMM orbital information used in this study, and how it has been used in the GCM. Section 3 introduces the CSU GCM, and explains how the experiment has been designed. Section 4 examines the satellite sampling frequency at annual, seasonal, monthly, and diurnal time scales, and compares the "satellite-observed" and "real" GCM precipitation and Outgoing Longwave Radiation (OLR). Section 5 gives a summary and conclusions.

2. TRMM orbital data

TRMM is a low-latitude satellite, orbiting at an altitude of about 350 km, with an orbital period of 91.5 minutes (15.7 orbits per day). Among the five remote-sensing instruments flown on TRMM, the TRMM Microwave Imager (TMI; Kummerow et al. 1997) and the Precipitation Radar (PR; Meneghini and Kozu 1990) provide measurements of rainfall. The Visible Infrared Scanner (VIRS) and the Clouds and the Earth's Radiant Energy System (CERES; Wielicki and Barkstrom 1991) sensors provide brightness temperatures and broadband radiative fluxes, respec-

tively. Table 1 lists some characteristics of these sensors. The TMI has a swath width of 758.5 km, about three times wider than that of the PR (220 km). Although the CERES radiometers can theoretically view an area as wide as 2000 km at the surface, the effective swath width for radiative fluxes is about 1200 km (Dr. Yong Xiang Hu, personal communication) due to the noise level at the edges of the orbit.

In this study, in order to examine sampling statistics for precipitation and OLR associated with the TRMM sensors on annual, seasonal, monthly, and diurnal time scales, we have analyzed TRMM data from the starting date, December 7 1997, to December 31 1999. The geolocations of pixel data at the center and two edges of the sensor orbits are saved. By simply assuming that a GCM grid box is viewed (not viewed) by the satellite if scans cover more than (less than or equal to) one half of the grid box, we are able to map the area “viewed” by the TRMM satellite onto the GCM grid boxes. Errors resulting from partial sampling of a grid box should become smaller as the size of the grid box becomes smaller, and are not considered in the current study. As shown in Figure 2, a satellite-sampling field corresponding to the GCM grid boxes is then constructed at 1-hour intervals for each sensor. The “viewed” and “unviewed” grid boxes are identified.

3. The CSU GCM and Experiment Design

The most recent version of the CSU GCM, which uses a new type of dynamic core (Ringler et al. 2000), is used in this study. A unique feature of the new dynamic core is that the model is discretized in the horizontal on a geodesic grid which is nearly uniform over the entire globe (Heikes and Randall 1995a, b). Such nearly uniform grids are especially useful for satellite sampling studies, compared to the conventional longitude-latitude grid. The vertical structure of the atmosphere is represented using 17 layers, extending from the surface up to 1 hPa. The lowest layer is the planetary boundary layer, while the top of the model extends to the stratopause. The time steps for “dynamics” and “physics” are 360 seconds, and 1 hour, respectively.

The CSU GCM uses a modified Arakawa-Schubert (1974) parameterization of convection developed by Randall and Pan (1993), Pan and Randall (1998), and Ding and Randall (1998). The parameterization is closed prognostically, and is also generalized to permit convection to originate at any and all model levels (except the top level) simultaneously. A bulk cloud microphysics

parameterization (Fowler et al. 1996, Fowler and Randall 1996a, b), which was originally developed for mesoscale models (Lin et al. 1983; Rutledge and Hobbs 1983, 1984), has been implemented into the GCM, to simulate stratiform cloud processes. The model also includes version 2 of the Simple Biosphere (SiB2) model of Sellers et al. (1996a, b) to simulate land-surface processes. The radiative transfer parameterization follows Harshvardhan et al. (1987). The CSU GCM has been tested, and evaluated against observations, and it is able to realistically simulate many important aspects of the climate (e.g. Randall et al. 1991; Fowler and Randall 1996a, b; Pan and Randall 1998; Ding and Randall 1998; Ringler et al. 2000; Lin et al. 2000).

Results are presented with a horizontal resolution based on 10242 polygons (approximately 225 km x 225 km), so that samplings of TMI, PR, VIRS and CERES can all be investigated. The simulation was started on January 1, and ran for two simulated years. Observed climatological monthly-mean sea surface temperature (SST) and sea ice distributions provide forcings for the model. Simulated and diagnosed fields at monthly-mean, seasonal-mean, and season-mean diurnal time scales have been constructed using "satellite-sampled" and "fully-sampled" GCM data. Data for regions of the western Pacific warm pool, the tropical eastern Pacific, the tropical Indian Ocean, the Amazon, etc., have been saved at 1-hour intervals.

4. Results

4a. Sampling frequency

Figure 3 shows the zonal-mean of the total number of overpasses for the different sensors on TRMM, for January. Note that this statistics is model-resolution-dependent. In the tropics, the monthly-mean sampling rates for TMI and VIRS are around 30 for each grid box (on the average about once per day), consistent with the pre-launch sampling studies of North (1988), Shin and North (1988), and Bell et al. (1990). The sampling rates for PR and CERES are about 10 and 50 respectively, demonstrating the significant impact of the sensor swath widths on the sampling frequencies. The sampling rates increase poleward and peak between 34° and 38° , near the edges of the satellite coverage. Overall, the monthly-mean and seasonal-mean sampling rates of TMI, PR, VIRS, and CERES are only about 4%, 1.3%, 4%, and 6.7% of the GCM sampling rate (744 times in January) in the Tropics.

Time series of TRMM samplings within January (Figure 4) further suggest that the TRMM satellite visits a given grid box in low latitudes neither randomly nor at constant intervals. The visit patterns are more complicated than those assumed in many earlier sampling studies, in which the visit intervals are nearly constant. Although riding on the same satellite, each TRMM sensor appears to have its own swath-width-related sampling frequency at the surface. As shown below, diurnal undersamplings associated with the satellite's orbital geometry and sensors' swath widths could generate spurious oscillations in the reconstructed monthly-mean fields, and this appears to be especially serious for sensors with narrower swath wide such as PR.

Figure 5 compares the diurnal sampling frequencies of the TRMM sensors within one month (solid lines), and three months (dashed lines) for three selected grid boxes at the same longitude but different latitudes (one near the equator, and the other two at 30°N and 30°S, respectively). For one month of TMI data, the grid box at 30°N has significantly more samples between 1900 and 0800 UTC compared to 0900-1800 UTC, while the grid box at 30°S at the same longitude has significantly more samples between 0800 and 1900 UTC, suggesting possible large sampling bias associate with the satellite's orbital geometry. As will be demonstrated in Section 4b, this will lead to more daytime samples (relative to nighttime samples) in one hemisphere and more nighttime samples (relative to daytime samples) in the other hemisphere. Similar biases may also exist in PR, VIRS, and CERES products when studying monthly means and diurnal variability using only one-month data. For grid boxes near the Equator, the samples within a month are more evenly distributed over each 1-h interval, even for sensors with narrow swath widths. As 3 months of TRMM data are accumulated, the 2.25°x 2.25° grid box can be sampled evenly for each 1-h interval without a clear sampling bias towards certain times of day, although this does not guarantee that the diurnal signals for various climate variables can be well captured. The seasonal-mean satellite diurnal sampling rates near the Equator for each 1-h interval are about 1 or 2 for PR, 4 for TMI and VIRS, and 7 for CERES from December to February , compared to 90 times for the GCM.

In summary, examination of the TRMM sampling rates indicates that sensor swath widths have significant impacts on sampling frequencies. The monthly-mean and seasonal-mean satellite sampling rates are about one or two orders smaller than the GCM sampling rate. For grid boxes

away from the Equator, there are large diurnal undersamplings associated with the satellite's orbital geometry, which may lead to more daytime samples relative to nighttime samples in one hemisphere, and more nighttime samples relatively to daytime samples in the other hemisphere when using only one month of TRMM data. This diurnal undersampling, as will be shown later, can bring significant biases to both monthly-mean fields and diurnal studies. In order to adequately sample diurnal variability, it is necessary to accumulate multiple months of TRMM pixel data onto a grid.

4b. Bias in monthly- and seasonal-means

Total precipitation rate and OLR are two important variables that are commonly used in climate studies and retrieved by TRMM. They have different diurnal variabilities, as well as different amplitude scales, and thus possibly different satellite sampling errors at seasonal-mean and seasonal-mean diurnal time scales.

One of the most important objectives of TRMM sampling studies is to evaluate the sampling bias of the inferred monthly-mean precipitation and radiative fluxes. Figure 6 compares the TMI- and PR-sampled with fully-sampled monthly-mean (January) GCM total precipitation. Their geographical distributions and zonal means are very similar. All of the large-scale features, including the InterTropical Convergence Zone (ITCZ) and rainfall maxima and minima in the tropics and subtropics, are very well sampled by TMI and PR. Area-mean differences are 0.02 and 0.03 mm day⁻¹ respectively, much less than the area-mean rain rate of 2.4 mm day⁻¹. However, a few grid boxes have differences larger than 2.0 mm day⁻¹. Due to smaller sampling rates associated with a narrower swath width, the PR-sampled total precipitation tends to have larger sampling errors than the TMI-sampled total precipitation, especially over the maritime continent and the western Pacific, the Amazon Basin, and the tropical Africa, where precipitation occurs frequently and has large diurnal variations.

In order to estimate the average amplitudes of differences between "satellite-sampled" and "fully-sampled" monthly-mean total precipitation, using two years of simulated data, we calculate the root-mean squares (RMSs) of TMI- and PR-sampled monthly-mean precipitation relative to the fully-sampled month-mean precipitation (Figure 7). The RMS plots indicate that the TRMM

sampling errors are positively correlated with precipitation amount and sensor swath widths, as noticed in previous sampling studies (e.g., Bell et al. 1990). The averaged TMI and PR sampling errors in the Tropics and midlatitudes, where deep convection dominates, are about 0.7 and 1.5 mm day⁻¹ respectively. The sampling errors in the subtropics, where convection seldomly occurs, are considerably smaller, especially over the oceanic regions west of main continents, and large desert areas such as the Sahara. Due to smaller monthly sampling rates and the large diurnal variability of precipitation in the Tropics, the PR-sampled precipitation has RMS errors two times larger than the TMI-sampled precipitation. By simply dividing the averaged RMS of total rain by averaged total rain rate, we can estimate that the TRMM TMI and PR relative sampling errors could be as large as 10 and 30% in the Tropics, and 20 and 40% in the subtropics, for zonally averaged monthly-mean rain rates. Monthly mean precipitation over individual grid boxes may have even larger relative sampling errors.

Figure 8 compares the VIRS- and CERES-sampled monthly-mean (January) OLR with the fully-sampled OLR between 40°S and 40°N. Again, the sampled OLR fields and their zonal means are very similar to the fully-sampled fields. The largest difference for a grid box is about 8 W m⁻² and therefore the largest deviation is less than 5% in the OLR field, if 160 W m⁻² is assumed to be the lowest monthly-mean OLR value in low latitudes. One interesting feature to notice is that both the VIRS- and CERES-sampled OLR are systematically lower (2-6 W m⁻²) than GCM OLR over the subtropical continents in the Northern Hemisphere, and higher than the GCM OLR over the subtropical continents in the Southern Hemisphere. The February OLR has also been examined, and the situation reverses (not shown). A possible explanation, as suggested by the monthly-mean diurnal sampling rates (Figure 5), is that in January (1998), TRMM tends to sample more nighttime situations in the Northern Hemisphere, and thus correspondingly more daytime situations in the Southern Hemisphere. Since the diurnal variation of OLR is stronger over the subtropical continents than over the oceans, the impact of this uneven diurnal sampling in two hemispheres is seen on the large landmasses in the subtropics.

Figure 9 shows the RMS errors of VIRS- and CERES-sampled monthly mean OLR. There appear to be two major factors contributing to RMS errors. Large RMS errors occur in the Tropics, where deep convection usually dominates. They are associated with diurnal undersampling of

tropical convection, and could be substantially reduced for sensors with wider swath widths. The CERES-sampled OLR has smaller RMS errors ($2-3 \text{ W m}^{-2}$) than the VIRS-sampled OLR ($3-5 \text{ W m}^{-2}$) in the Tropics. Large RMS errors over the subtropical continents, where precipitation seldomly occurs, are mainly related to uneven day and night samplings between the hemispheres in each month due to TRMM's orbital geometry. Both VIRS- and CERES-sampled OLR show similar order-of-magnitude RMS errors over the subtropical continents ($3-6 \text{ W m}^{-2}$). Such uneven samplings of daytime and nighttime in the subtropics have almost no effects on the precipitation fields, since precipitation seldom falls over the subtropical continents and its day-night variations are small. Over the subtropical oceans west of the major continents, where clear-skies and/or stratus clouds dominate, the RMS values are generally less than 1.5 W m^{-2} and the OLR patterns can be well captured by one month of TRMM data. Overall, most grid boxes within the TRMM region have RMS errors smaller than 6 W m^{-2} . Therefore, the TRMM satellite relative sampling errors are generally smaller than 5% for the monthly-mean OLR.

4c. Tropical means

Tropical means and tropical-mean anomalies of precipitation and radiation fluxes are valuable measures of the sensitivity of the tropical hydrologic cycle to El Nino-Southern Oscillation (ENSO), and of the skills of models' predictability. Soden (2000), using satellite observations of temperature, water vapor, precipitation, and longwave fluxes, characterized the variations of the tropical hydrologic and energy budgets associated with ENSO. He found that although multi-model ensemble-mean simulations can realistically reproduce changes in the observed tropospheric temperature, water vapor, and OLR, changes in model-predicted precipitation and surface net longwave flux are substantially smaller than observed. There are concerns that such discrepancies may come partly from errors in satellite observations and partly from a fundamental error that is common to all GCMs (Soden 2000).

Although the current study is not able to determine whether the satellite retrievals overestimate the amplitude of interannual variability, we are able to examine the role of TRMM sampling errors in constructing the seasonal changes of the tropical hydrologic cycle and radiative fluxes. Figure 10 shows the fully- and TRMM-sampled GCM annual cycle of tropical precipita-

tion and OLR (Fig. 10a) and their deviations (Fig. 10b) over three different tropical belts (10°N - 10°S , 20°N - 20°S , 30°N - 30°S) using monthly-mean averages. Although amplitudes become smaller as the averaging areas become larger, the time series of tropical-mean precipitation and OLR deviations clearly indicate spurious low-frequency oscillations associated with TRMM's orbital geometry, with periods ranging from 3 to 4 months. While the relative fluctuations of the sampled-OLR are negligible, the relative fluctuations of the sampled-precipitation are about 1-2%, about one-third of satellite-derived long-term oceanic precipitation fluctuations as derived by Soden (2000). This number is quite significant considering that the relative fluctuation of precipitation is even larger for averages over ocean-only regions.

Figure 11 shows TMI-sampled tropical-mean GCM total precipitation deviation (from fully-sampled total precipitation) as derived from daily values (Fig. 11a), along with the observed TMI daily precipitation (Fig. 11b). All the deviation plots indicate that there are strong oscillations on 23-day period in tropical-mean daily precipitation anomalies, which are due to that the TRMM orbit precession relative to the Sun direction has a 46-day cycle (Dr. Kummerow, personal communication). Such spurious oscillations have similar magnitudes (about 0.5 mm day^{-1} between 20°N and 20°S) to the satellite-observed precipitation oscillation (about 1.6 mm day^{-1}). The 3-4 month oscillations shown in Figure 10, in which monthly-mean values are used, may be examples of aliasing from the 23-day oscillations. This shows that caution must be used when applying satellite observations of tropical-mean precipitation to interpret climate variations and/or evaluate climate simulations at intraseasonal and interannual scales.

4d. Frequency and intensity

Although frequency and intensity of precipitation are important variables in climate diagnostics and simulations and have been receiving more and more attentions (Petty 1995; Chen et al. 1996; Petty 1997; Dai 2000), they are rarely evaluated in satellite sampling studies due to the lack of data. Rainfall on a specific grid box is not continuous over time, and the monthly- or seasonal-mean rain rate is typically computed as the accumulated rain amount from each observation divided by total number of observations. The mean rain rate does not tell the distributions of intensity and frequency of rain events within an individual month. For example, it is possible that

a region characterized of light rain with high frequency has the same monthly-mean rain rate as a region characterized of heavy rain with low frequency.

Figure 12 illustrates the correlation between seasonal-mean rain amount and rain incidence from GCM and TMI for the entire TRMM region and for different climate regimes. GCM rain incidence is defined as total rainy hours divided by total hours, while TMI-sampled rain incidence is defined as total rainy hours sampled by TMI divided by total hours sampled by TMI. Over the entire TRMM region (between 40°N and 40°S), GCM results indicate that there is a general trend for regions having larger rain incidence to have larger rain amounts. The TMI-sampled results can capture this general increasing trend. Over the western Pacific warm pool, and the summer Amazon Basin, where deep convection usually dominates, the TMI-sampled results agree well with the GCM results and the scattering is similar; most grid boxes are characterized of large rain amount with high rain incidence. Hawaii is characterized by light rain, The fully- and TMI-sampled GCM results agree very well and indicate that the mean rain rate over Hawaii is below 4 mm day⁻¹, and precipitation falls less than 20% of total observations. The eastern Pacific ocean is in the subsidence region of the Walker circulation and usually dominated by clear sky situations and shallow stratus or cumulus clouds. Both fully- and TMI-sampled GCM results show very light precipitation over the eastern Pacific with rain incidence ranging from 0 to 20%, consistent with Petty (1995)'s observations, based on shipboard weather reports, that drizzle is the preferred form of precipitation over persistent marine stratus and stratocumulus areas in the subtropical highs.

Figure 13 shows the probability density distribution of precipitation for a 2.25°x2.25° grid box over the summer Amazon Basin, the western Pacific warm pool, the maritime continent, and the eastern Pacific Ocean. Over the Amazon Basin where convection frequently occurs, light rain events with rain rate below 0.5 mm day⁻¹ dominate and are about 20-30% of the total rain events. Other rain event frequencies, starting from 5% for rain rates between 0.5 and 1.0 mm day⁻¹, gradually decrease as rain rate becomes larger. The TMI-sampled rain event frequency in general agrees well with fully-sampled rain event frequency, especially at low-rainrate ranges. At high rainrate ranges, satellite observations may slightly overestimate or underestimate precipitation frequency due to inadequate sampling. The fully- and TMI-sampled rain events over the warm

pool and maritime continents indicate similar features, except that rain event frequency for rain rate below 0.5 mm day^{-1} is about 14% of total rain events. The eastern Pacific Ocean is characterized by clear sky and shallow stratus clouds. Precipitation events, if there are any, are mostly light rain events. Satellite observations from TRMM can accurately capture these features.

Figure 14 shows the probability density distribution of OLR for a $2.25^\circ \times 2.25^\circ$ grid box over the summer Amazon Basin, the western Pacific warm pool, the maritime continent, and the eastern Pacific. Fully-sampled OLR tends to have frequency maxima between 200 and 240 W m^{-2} over the Amazon, 200 W m^{-2} over the warm pool and maritime continent, respectively. VIRS-sampled OLR, if smoothed, can well capture the broad features over these deep convective regions. Over the eastern Pacific, fully- and VIRS-sampled OLR agree with each other very well since stable condition prevails over this region. Both of them show a double peak structure with the major frequency peak (36%) associated with clear sky situation at 290 W m^{-2} , and the secondary peak (16%) probably associated with shallow stratus clouds at about 260 W m^{-2} .

4e. Bias in the seasonal-mean diurnal cycle

Numerous observations have shown that the diurnal variation of convection is generally stronger over land than over oceans, and that the strongest convection over the summer continents such as the Amazon Basin usually occurs in the late afternoon or early evening, due to dominant daytime boundary layer heating (e.g., Wallace 1975; Gray and Jacobson 1977; Short and Wallace 1980; Kousky 1980; Meisner and Arkin 1987; Liebmann and Gruber 1988; Hartmann et al. 1991; Lin et al. 2000). Lin et al. (2000) examined the CSU GCM-simulated diurnal variability of the hydrologic cycle and radiative fluxes over the Amazon Basin. They found that the CSU GCM can capture many aspects of the observed diurnal cycle of convection, although there are 2-3 hour lags in peak precipitation and OLR relative to observations. In this subsection we examine the sampled Amazon diurnal cycle for an individual grid box, and also averaged over the entire Amazon Basin.

Figure 15 compares the fully-, and TRMM-sampled GCM seasonal-mean diurnal cycles of total precipitation and OLR for a grid box at the center of the Amazon. Each $2.25^\circ \times 2.25^\circ$ grid box is sampled by the satellite on the average 3-4 times for TMI, 1-2 times for PR, 4 times for

VIRS, and 6 times for CERES for each 1-h interval within a single season, compared to about 90 times within the GCM. The diurnal cycle of the GCM precipitation (Fig. 15a) shows a maximum (20 mm day^{-1}) at 1800 LST, and a minimum (8 mm day^{-1}) in the morning between 0900 LST and 1100 LST. The diurnal cycle of OLR (Fig. 15b) shows a maximum at 0900 LST and a minimum at 1800 LST. The TMI-sampled precipitation and VIRS-sampled OLR time series show large deviations for most 1-h intervals, due to inadequate samplings. Maxima and minima in precipitation and OLR can even shift their timings.

By averaging over a large area with relatively uniform diurnal signals, the diurnal sampling can be significantly improved. Figure 16 compares the fully-sampled and TRMM-sampled GCM seasonal-mean diurnal cycle of total precipitation and OLR over the Amazon Basin (ensembles of 65 grid boxes). The differences between fully-sampled and TRMM-sampled at each 1-hour intervals became much smaller than those computed for one grid box, and daily maxima and minima in total precipitation and OLR are well captured by the simulated satellite (within 1-2 hours).

5. Summary and Conclusions

Remote sensing data from the TRMM satellite have for the first time provided comprehensive and synchronous measurements of precipitation and radiative fluxes in the Tropics and subtropics. TRMM data will be extensively used to study natural variability on the annual, seasonal, and composited diurnal time scales, and to evaluate climate models' skills in predicting climate changes. The TRMM satellite typically visits an area the size of a GCM grid box about once a day or less, and the constructed fields on different temporal and spatial scales may suffer large uncertainties due to inadequate samplings and intrinsic factors embedded in the satellite's orbital geometry. A number of sampling studies of TRMM precipitation were conducted before launch but most rainfall statistics were derived over very limited regions in the Tropics within short time periods. The satellite sampling impacts on the measured tropical hydrologic cycle and radiative energy budgets, which are very valuable for accurately monitoring climate variations and evaluating climate simulations, are difficult to estimate due to the lack of data.

By incorporating the TRMM orbital information in the geodesic version of the CSU GCM, we are able to "fly" a satellite in the GCM, and sample the simulated atmosphere the same way as

TRMM samples the real atmosphere. The TRMM sampling errors on interannual, intraseasonal, monthly, and composited diurnal time scales can then be inferred by directly comparing fully-sampled GCM atmosphere with TRMM-sampled GCM atmosphere.

There are four sensors aboarding TRMM measuring precipitation, brightness temperatures, and radiative fluxes, respectively. Sampling frequency analyses indicate that the sensors' swath widths have significant impact on the sampling rates. TMI and VIRS sample each $2.25^{\circ} \times 2.25^{\circ}$ grid box in the tropics and subtropics about once per day but at different local times everyday while PR and CERES visit each grid box about once every three days and twice per day, respectively. Besides inadequate samplings resulting from the sensors' swath widths, there are large diurnal undersamplings associated with TRMM's orbital geometry for grid boxes away from the equator. This diurnal undersampling leads to more daytime samples relative to nighttime samples in one hemisphere, and more nighttime samples relative to daytime samples in the other hemisphere when only one month of TRMM data are used. These sampling problems, if not carefully managed, could bring significant biases to constructed climate fields on various temporal and spatial scales, and may interfere with climate monitoring.

The sampling errors in OLR and precipitation monthly means are calculated based on a two-year simulation. The VIRS- and CERES-sampled GCM OLR monthly means are very similar to the fully-sampled GCM OLR, and are able to capture all the large-scale features in the Tropics and subtropics. There are two major factors contributing to RMS errors in sampled OLR monthly means. RMS errors ($3-5 \text{ W m}^{-2}$) located in the Tropics, where deep convection usually dominates, are associated with inadequate temporal sampling of tropical convection, and can be substantially reduced for sensors with wider swath widths. RMS errors ($3-6 \text{ W m}^{-2}$) over the subtropical continents, where precipitation seldom falls, are mainly related to uneven samplings of daytime and nighttime situations in two hemispheres within individual months due to TRMM's orbital geometry. Both VIRS- and CERES-sampled OLR show similar order of magnitude of RMS errors over the subtropical continents. Overall, the largest OLR difference for a grid box is about 8 W m^{-2} and therefore the largest deviation is less than 5% in the OLR field, if 160 W m^{-2} is assumed to be the lowest monthly-mean OLR value. Although there are sampling errors associated with inadequate sampling resulting from sensor swath widths and diurnal undersampling resulting from TRMM's orbital geometry, the OLR monthly- and seasonal-means are not sensitive to these sampling errors

by TRMM. This is mainly because of the relatively large OLR values (on the order of 10^2 W m^{-2}) and insignificant diurnal variability compared to precipitation (ranging between 0 and 10 mm day^{-1} or larger). Therefore, both monthly mean and seasonal mean OLR can be well sampled by VIRS and CERES.

TMI- and PR-sampled monthly-mean precipitation can also capture all the large-scale features in the Tropics and subtropics. However, due to smaller sampling rates associated with a narrower swath width, PR-sampled total precipitation tends to have larger difference than the TMI-sampled total precipitation. TMI and PR relative sampling errors are estimated to be as large as 10 and 30% in the Tropics, and 30 and 40% in the subtropics, for zonally averaged monthly-mean rain rates.

Correlations between rain amount and rain intensity, as well as probability density function of precipitation and OLR are also investigated over different climate regimes using seasonal-mean data. TRMM-sampled data agree well with fully-sampled data, especially over the eastern Pacific where stable conditions prevail.

TMI and VIRS sample each $2.25^\circ \times 2.25^\circ$ grid box in the tropics and subtropics about 3 times for each 1-h interval within a single season. With so few samples, the seasonal-mean diurnal cycles of precipitation and OLR cannot be well captured for one grid box. Maxima and minima in rainfall and OLR may even shift significantly. By accumulating the satellite data for a long enough period (seasonal ensembles for a few years), and/or by averaging the data over a large area with relatively uniform diurnal signals, the diurnal cycles of precipitation and OLR can be well sampled at 1-h intervals for $2.25^\circ \times 2.25^\circ$ grid boxes.

Tropical means and tropical-mean anomalies of precipitation and radiation fluxes are valuable measures of the sensitivity of the tropical hydrologic cycle to ENSO, and of the skills of models' predictability. The TRMM sampling impact on tropical mean hydrologic cycle and radiative fluxes are also evaluated. There are strong spurious oscillations associated with TRMM's orbital geometry, with periods of 23 days and 3-4 months, in tropical-mean daily and monthly precipitation. While the relative fluctuations of the sampled-OLR are negligible, the relative fluctuations of the sampled precipitation are of the same order of magnitude as the observed climate variability. Caution must be used when applying TRMM observations of tropical-mean precipitation to interpret climate variations at intraseasonal and interannual scales.

Satellite data, along with other data, are commonly assimilated into operational model reanal-

yses to provide better forecasting and monitoring of daily weather changes, and are extensively used to evaluate long-term climate simulations. This is useful because satellites can view large areas where in-situ observations are not available. However, large, spurious low-frequency signals can result from satellite sampling. If not carefully managed, these errors can easily contaminate the inferred climate fields at various temporal and spatial scales.

Acknowledgments

The TRMM data were provided by the NASA Goddard Space Flight Center Data Archive and Distribution Center. Many thanks to Drs. Chris Kummerow, Ye Hong, and Song Yang for help on TRMM data processing. Thanks to Mr. Donald Dazlich and Dr. Charlotte Demott for help on the CSU GCM. Special thanks to Dr. Tom Bell for providing much valuable insights and critical comments to an early version of the manuscript. This research has been supported by NASA, grants NAG5-4749 and NAS1-98125.

Figure Legends

Figure 1: A schematic showing how to investigate satellite sampling issue with the help of a GCM.

Figure 2: Simulated orbits for TMI, PR, VIRS and CERES on the geodesic version of the CSU GCM. The black belts represent the areas viewed by the TRMM sensors during the first two hours of the simulation.

Figure 3: Zonal means of sampling frequencies for TMI, PR, VIRS, and CERES in January, 1998 between -40° and 40° .

Figure 4: Time series of samples of TMI, PR, VIRS, and CERES within January 1998 on a random $2.25^{\circ} \times 2.25^{\circ}$ grid box in the Tropics.

Figure 5: Diurnal time series of sampling rates of TMI, PR, VIRS, and CERES within one month, and three months for three selected grid boxes at the same longitude but different latitudes (one near the equator, and the other two at 30°N and 30°S , respectively).

Figure 6: Horizontal distributions, and zonal means of fully-sampled, TMI- and PR-sampled precipitation, and their differences (in unit of mm day^{-1}).

Figure 7: Horizontal distributions, and zonal means of root-mean-square differences between satellite-sampled and fully-sampled total precipitation (in units of mm day^{-1}).

Figure 8: Horizontal distributions, and zonal means of fully-sampled, VIRS- and CERES-sampled OLR, and their differences (in unit of W m^{-2}).

Figure 9: Horizontal distributions, and zonal means of root-mean-square differences between satellite-sampled and fully-sampled OLR (in units of W m^{-2}).

Figure 10: Tropical means (a) and tropical mean deviations (b) of precipitation (mm day^{-1}) and OLR (W m^{-2}) between 10°N and 10°S , 20°N and 20°S , 30°N and 30°S .

Figure 12: Correlation between monthly-mean rain rates and rain incidence over the different climate regimes in the Tropics for fully- and TMI-sampled precipitation.

Figure 13: Probability density function of fully- and TMI-sampled rain events over the Amazon Basin, the western Pacific warm pool, the maritime continent, and the eastern Pacific.

Figure 14: Probability density function of fully- and TMI-sampled OLR over the Amazon Basin, the western Pacific warm pool, the maritime continent, and the eastern Pacific.

Figure 15: Seasonal-mean diurnal time series of fully- and TRMM-sampled GCM precipitation and OLR on a grid box in Amazon.

Figure 16: Seasonal-mean diurnal time series of fully- and TRMM-sampled GCM precipitation and OLR averaged over the Amazon.

Reference

- Arakawa, A, and W. H. Schubert, 1974: Interaction of a cumulus cloud ensemble with the large-scale environment,. Part I. *J. Atmos. Sci.*, 31, 674-701.
- Bell, T. L., 1987: A space-time stochastic model of rainfall for satellite remote-sensing studies. *J. Geophys. Res.*, 92, 9631-9643.
- Bell, T. L., A. Abdullah, R. L. Martin, and G. R. North, 1990: Sampling errors for satellite-derived tropical rainfall: Monte Carlo study using a space-time stochastic model. *Journal of Geophysical Research*, 95, 2195-2205.
- Bell, T. L., and N. Reid, 1993: Detecting the diurnal cycle of rainfall using satellite observations. *J. Appl. Meteor.* 32, 311-322.
- Bell, T. L., and P. K. Kundu, 1996: A study of the sampling error in satellite rainfall estimates using optimal averaging of data and a stochastic model. *J. Climate*, 9, 1251-1268.
- Bell, T. L., P. K. Kundu, and C. D. Kummerow, 1997: Sampling errors for gridded rainfall averages obtained from low-earth orbiting satellites. 9-12, The AMS Conference on Hydrology, Long Beach, California, 2-7 February 1997.
- Bell, T. L., and P. K. Kundu, 2000: Dependence of satellite sampling error on monthly averaged rain rates: Comparison of simple models and recent studies. *Journal of Climate*, 13, 449-462.
- Chen, M., R. E. Dickinson, X. Zeng, A. N. Hahmann, 1996: Comparison of precipitation observed over the continental United States to that simulated by a climate model. *J. Climate*, 9, 2233-2249.
- Dai, A., 2000: Global precipitation and thunderstorm frequencies. Part I: Seasonal and interannual variations. *J. Climate*, in press.
- Ding, P, and D. A. Randall, 1998: A cumulus parameterization with multiple cloud base levels. *Journal of Geophysical Research*, 103, 11341-11353.

Engelen, R. J., L. D. Fowler, P. J. Gleckler, and M. F. Wehner, 2000: Sampling strategies for the comparison of climate model calculated and satellite observed brightness temperatures. *Journal of Geophysical Research*, 105, 9393-9406.

Fowler, L. D., D. A. Randall, and S. A. Rutledge, 1996: Liquid and ice cloud microphysics in the CSU General Circulation Model. Part I: Model description and simulated microphysical processes. *J. Climate*, 9, 489-529.

Fowler, L. D., and D. A. Randall, 1996a: Liquid and ice cloud microphysics in the CSU General Circulation Model. Part II: Simulation of the earth's radiation budget. *J. Climate*, 9, 530-560.

Fowler, L. D., and D. A. Randall, 1996a: Liquid and ice cloud microphysics in the CSU General Circulation Model. Part III: Sensitivity tests. *J. Climate*, 9, 561-586.

Fowler, L. D., B. A. Wielicki, D. A. Randall, M. D. Branson, G. G. Gilbson, and F. M. Denn, 2000: Use of a GCM to explore sampling issues in connection with satellite remote sensing of the Earth's radiation budget. *Journal of Geophysical Research*, 105, 20757-20772.

Gray, W. M., and R. W. Jacobson, 1977: Diurnal variation of deep cumulus convection. *Mon. Wea. Rev.*, 105, 1171-1188.

Harshvardhan, R. Davies, D. A. Randall, and T. G. Corsetti, 1987: A fast radiation parameterization for atmosphere general circulation models. *J. Geophys. Res.*, 92, 1009-1942.

Hartmann, D. L., K. Kowalewsky, and M. L. Michelsen, 1991: Diurnal variations of outgoing longwave radiation and albedo from ERBE scanner data. *J. Climate*, 4, 598-617.

Heikes, R., and D. A. Randall, 1995a: Numerical integration of the shallow-water equations on a twisted icosahedral grid. Part I: Basic design and results of tests. *Mon. Wea. Rev.*, 1995, 123, 1862-1880.

Heikes, R., and D. A. Randall, 1995b: Numerical integration of the shallow-water equations on a twisted icosahedral grid. Part II: A detailed description of the grid and an analysis of numerical accuracy. *Mon. Wea. Rev.*, 1995, 123, 1881-1887.

- Huffman, G. J., 1997: Estimates of root-mean-square random error for finite samples of estimated precipitation. *J. Appl. Meteor.*, 36, 1191-1201.
- Kidder, S. Q., and T. H. Vonder Harr, 1995: Satellite Meteorology: An Introduction. *Academic Press*, 466pp.
- Kousky, V. E., 1980: Diurnal rainfall variation in Northeast Brazil. *Mon. Wea. Rev.*, 108, 488-498.
- Kummerow, C., W. S. Olson, and L. Giglio, 1997: A simplified scheme for obtaining precipitation and vertical hydrometeor profiles from passive microwave sensors. *IEEE Transactions on Geoscience and Remote Sensing*, 48, 5-411.
- Leith, C. E., 1973: The standard error of time-average estimates of climate means. *J. Appl. Meteor.*, 12, 1066-1069.
- Li, Q, R. L. Bras, and D. Veneziano, 1996: Analysis of Darwin rainfall data: Implications on sampling strategy. *J. Appl. Meteorology*, 35, 372-385.
- Liebmann, B., and A. Gruber, 1988: The annual variation of the diurnal cycle of outgoing long-wave radiation. *Mon. Wea. Rev.*, 116, 1659-1670.
- Lin, X. L. D. Fowler, and D. A. Randall, 2000: Use of a GCM to examine the credibility of TRMM satellite-sampled rainfall and radiative fluxes at seasonal-mean and seasonal-mean diurnal time scales. *Journal of Climate*, 13, 4159-4179.
- Lin, Y.-L., R. D. Farley, and H. D. Orville, 1983: Bulk parameterization of the snow field in a cloud model. *J. Climate Appl. Meteor.*, 22, 1065-1092.
- MaConnell, A., and G. R. North, 1987: Sampling errors in satellite estimates of tropical rain. *J. Geophys. Res.*, 92, 9567-9570.
- Meisner, B. N., and P. A. Arkin, 1987: Spatial and annual variations in the diurnal cycle of large-scale tropical convective cloudiness and precipitation. *Mon. Wea. Rev.*, 115, 2009-2032.
- Meneghini, R., and T. Kozu, 1990: Spaceborne Weather Radar. Artech House, 199pp.

North, G. R., 1988: Survey of sampling problems for TRMM. 337-348, *Tropical Rainfall Measurements*, Edited by J. S. Theon and N. Fugono.

Pan, D.-M., and D. A. Randall, 1998: A cumulus parameterization with a prognostic closure. *Quart. J. Roy. Meteor. Soc.*, 124, 949-981.

Petty, G. W., 1997: An intercomparison of oceanic precipitation frequencies from 10 special sensor microwave/imager rain rate algorithms and shipboard present weather reports. *J. G. R.*, 102, 1757-1777.

Petty, G. W., 1995: Frequencies and characteristics of global oceanic precipitation from shipboard present-weather reports. *BAMS*, 76, 1593-1616.

Randall, D. A., Harshvardhan, D. A. Dazlich, 1991: Diurnal variability of the hydrologic cycle in a general circulation model. *J. Atmos. Sci.*, 48, 40-62.

Randall, D. A. and D.-M. Pan, 1993: Implementation of the Arakawa-Schubert cumulus parameterization with a prognostic closure. *The Representation of Cumulus Convection in Numerical Models*, K. Emanuel and D. Raymond, Eds. *Metero. Monogr.*, 24, pp. 137-144.

Ringler, T. D., R. Heikes, and D. A. Randall, 2000: Modeling the atmospheric general circulation using a spherical geodesic grid: A new class of dynamic cores. *Mon. Wea. Rev.*, 128, 2471-2490.

Rutledge, S. A., and P. V. Hobbs, 1983: The mesoscale and micro-scale structure and organization of clouds and precipitation in midlatitude cyclones. VIII: A model for the "seeder-feeder" process in warm-frontal rainbands. *J. Atmos. Sci.*, 40, 1185-1206.

Rutledge, S. A., and P. V. Hobbs, 1984: The mesoscale and micro-scale structure and organization of clouds and precipitation in midlatitude cyclones. XII: A diagnostic modeling study of precipitation development in narrow cold-frontal rainbands. *J. Atmos. Sci.*, 41, 2949-2972.

Salby, M. L., 1988: Asynoptic sampling considerations for wide-field-of-view measurements of outgoing radiation, Part 1: Spatial and temporal resolution. *J. Atmos. Sci.*, 45, 1176-1183.

- Salby, M. L., and P. Callaghan, 1997: Sampling error in climate properties derived from satellite measurements: consequences of undersampled diurnal variability. *J. Climate*, 10, 18-36.
- Sellers, P. J., D. A. Randall, G. J. Collatz, J. Berry, C. Field, D. A. Dazlich, C. Zhang, and L. Bounoua, 1996: A revised land-surface parameterization (Sib2) for atmospheric GCMs. Part 1: Model formulation. *J. Climate*, 9, 676-705.
- Sellers, P. J., S. O. Los, C. J. Tucker, C. O. Justice, D. A. Dazlich, G. J. Collatz, and D. A. Randall, 1996: A revised land-surface parameterization (Sib2) for atmospheric GCMs. Part 2: The generation of global fields of terrestrial parameters from satellite data. *J. Climate*, 9, 706-737.
- Shin, K., and G. R. North, 1988: Sampling error study for rainfall estimate by satellite using a stochastic model. *J. Appl. Meteor.*, 27, 1218-1231.
- Short, D. A., and J. M. Wallace, 1980: Satellite-inferred morning-to-evening cloudiness changes. *Mon. Wea. Rev.*, 108, 1160-1168.
- Simpson, J., R. F. Adler, and G. R. North, 1988: Proposed tropical rainfall measuring mission (TRMM) satellite. *Bull. Amer. Meteor. Soc.*, 69, 278-295.
- Simpson, J., C. Kummerow, W.-K. Tao, and R. F. Adler, 1996: On the Tropical Rainfall Measuring Mission (TRMM). *Meteorol. Atmos. Phys.*, 60, 19-36.
- Soden, B. J., 2000: The sensitivity of the tropical hydrological cycle to ENSO. *J. Climate*, 13, 538-549.
- Soman V. V., J. B. Valdes, and G. R. North, 1995: Satellite sampling and the diurnal cycle statistics of Darwin rainfall data. *J. Appl. Meteor.*, 34, 2481-2490.
- Wallace, J. M., 1975: Diurnal variations in precipitation and thunderstorm frequency over the conterminous United States. *Mon. Wea. Rev.*, 103, 406-419.

3:04:59, March 2, 2001

Wielicki, B. A., and B. R. Barkstrom, 1991: Clouds and the Earth's Radiant Energy System (CERES): An earth observing system experiment. *Proc. Second Symp. Global Climate Change Studies*, New Orleans, LA, *Amer. Meteor. Soc.*, 11-16.

Zeng, L, and Levy, G., 1995: Space and time aliasing structure in monthly mean polar-orbiting satellite data. *J. G. R.*, 100, 5133-5142.

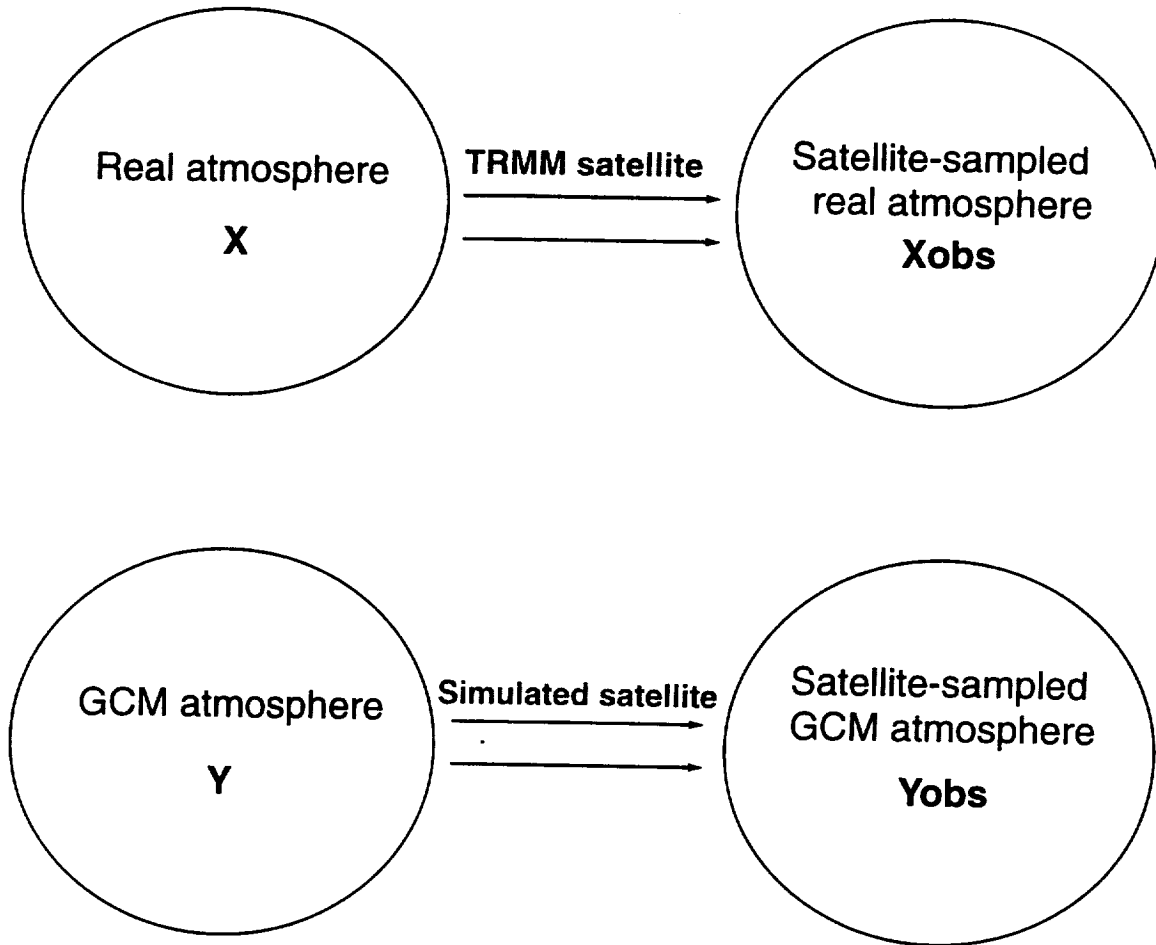


Figure 1

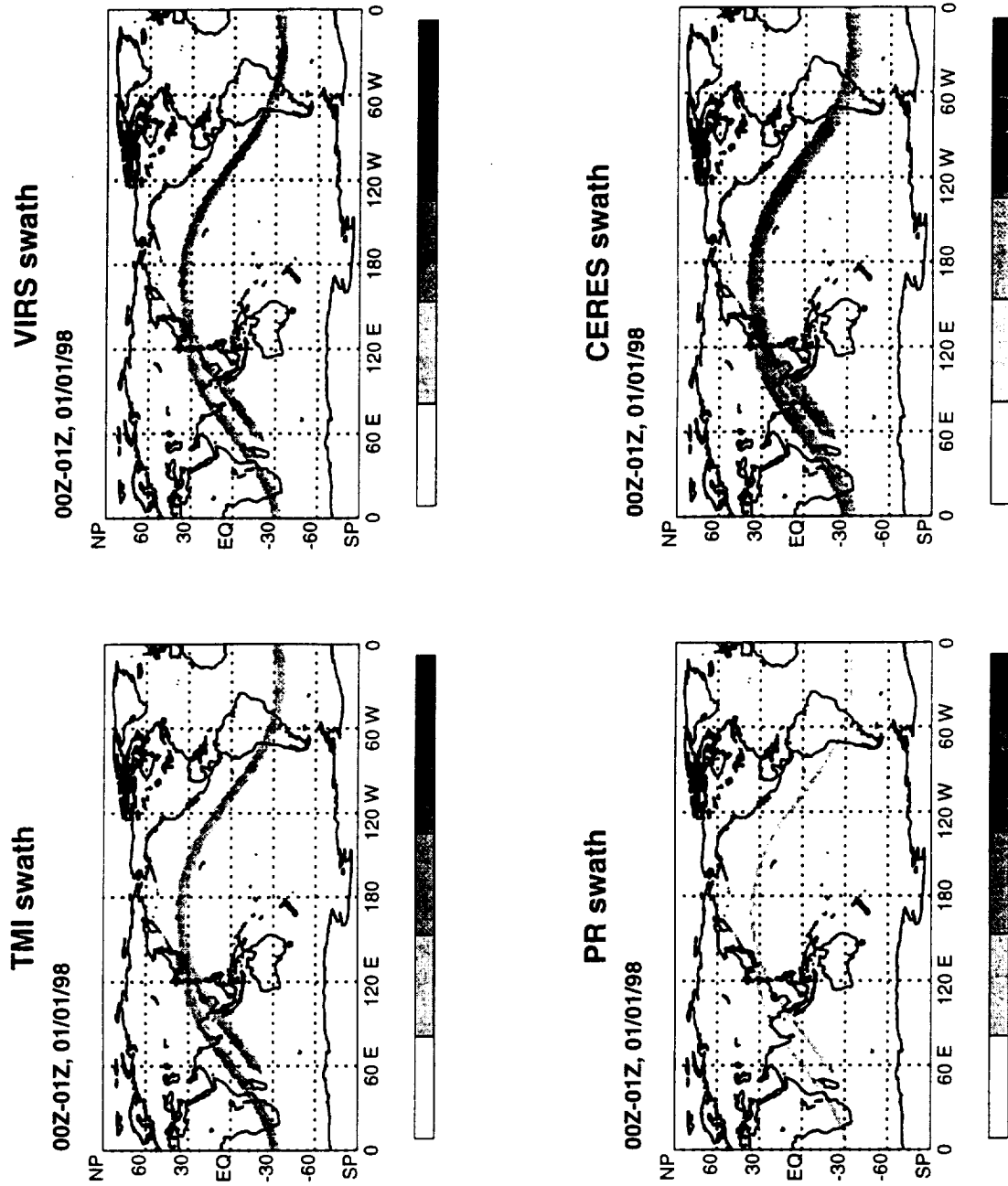


Figure 2

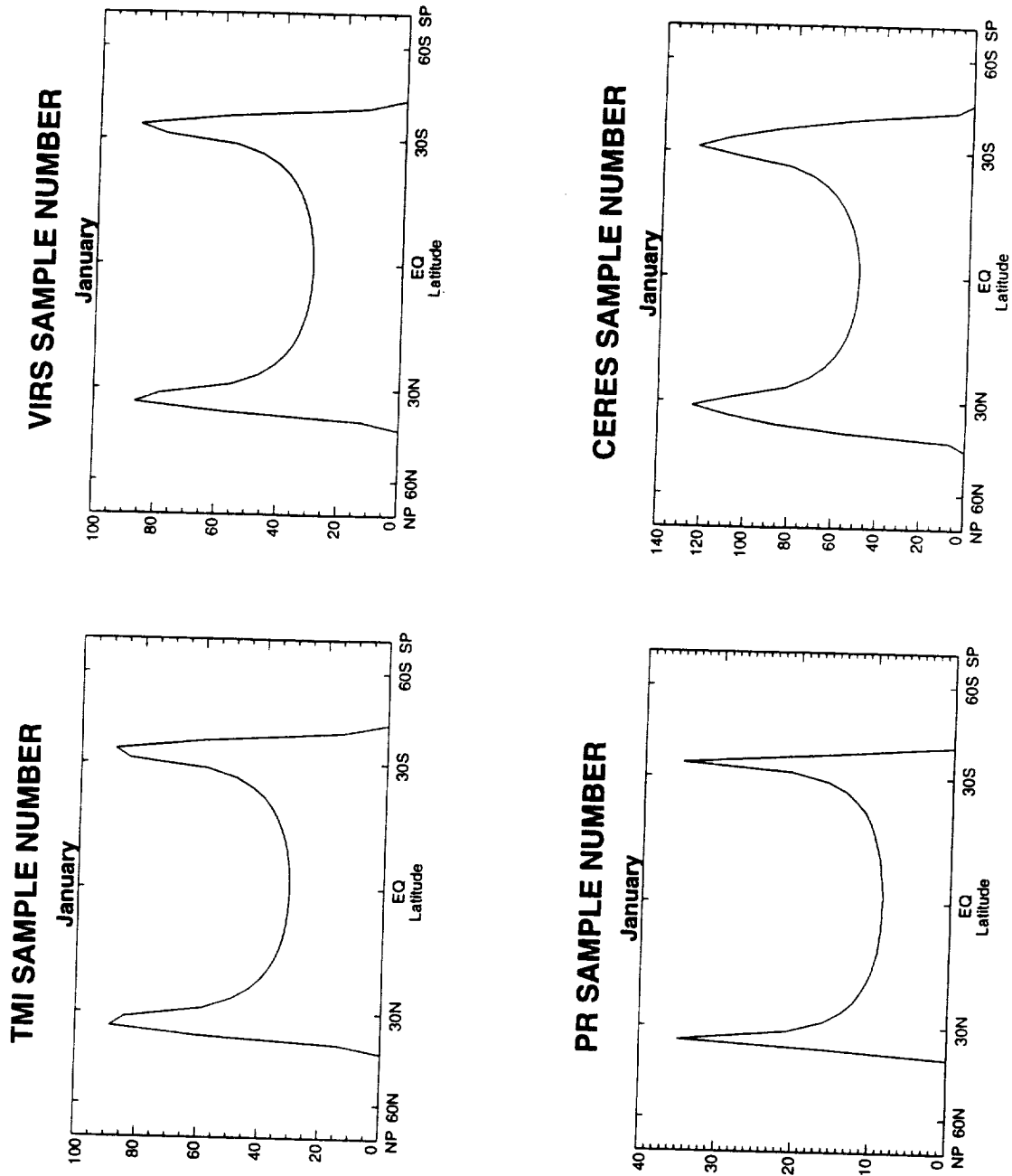


Figure 3



Figure 4

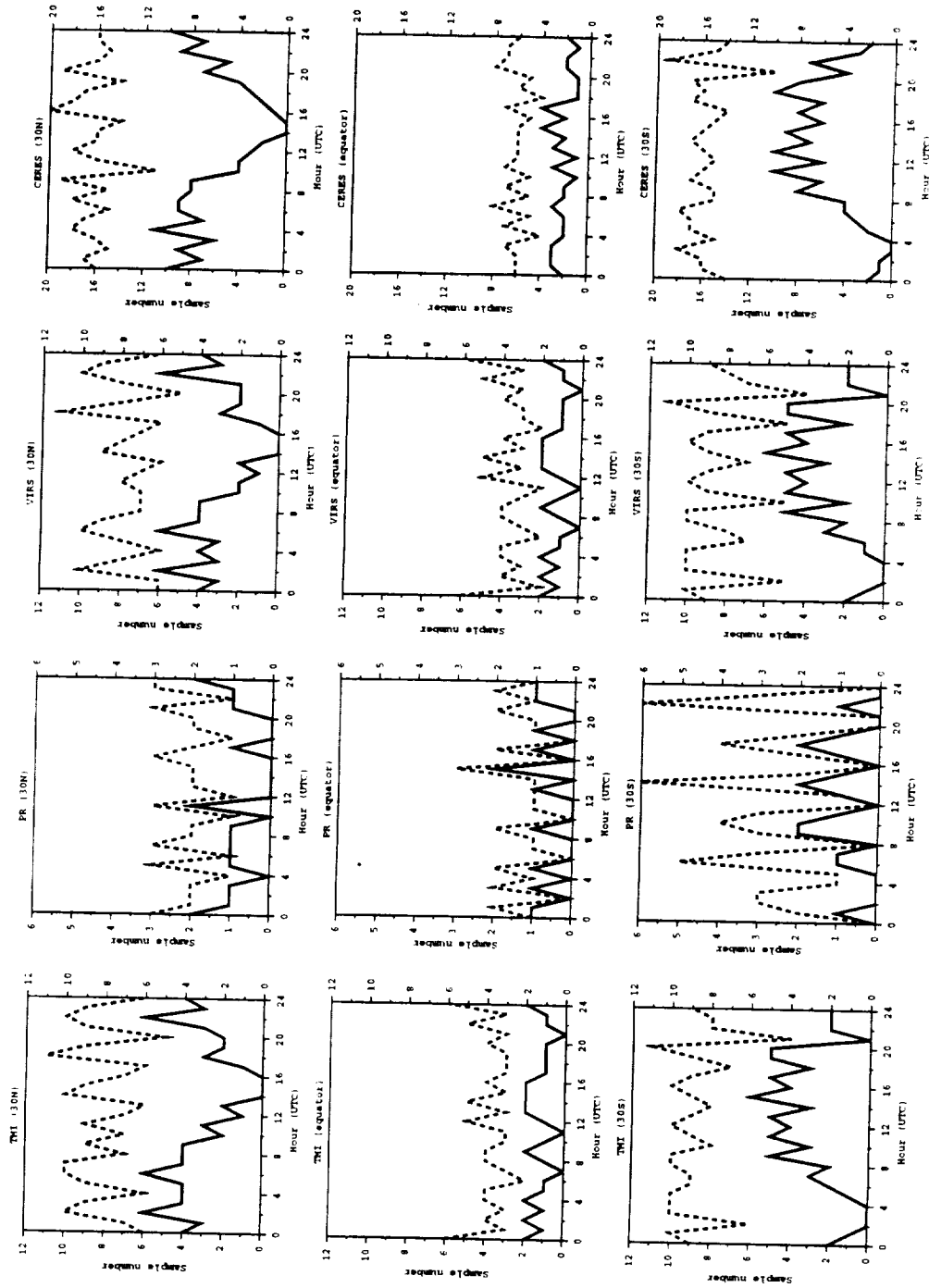


Figure 5

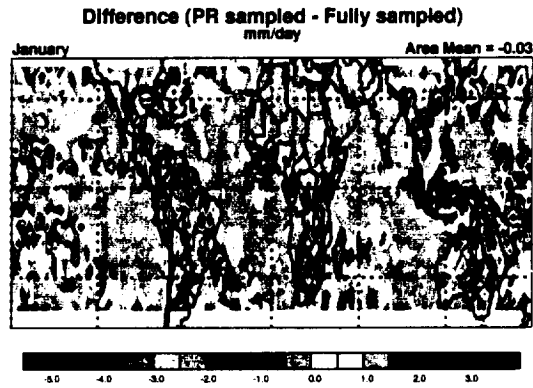
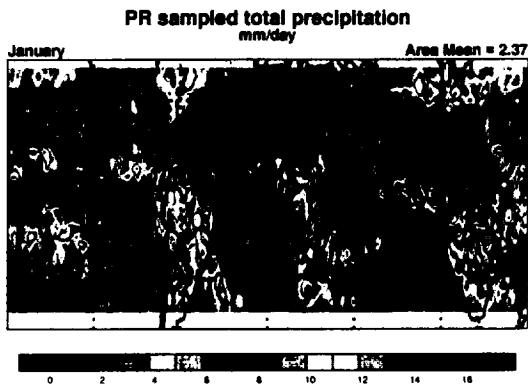
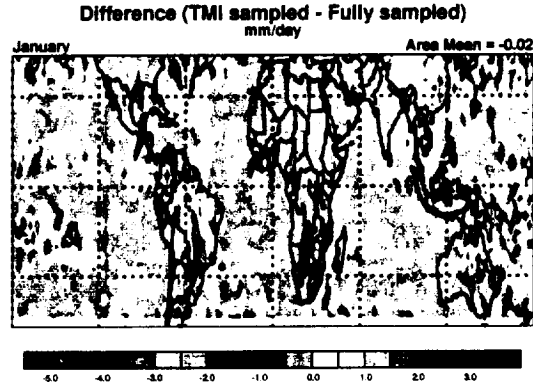
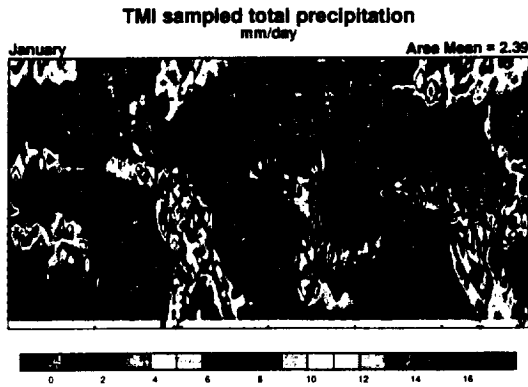
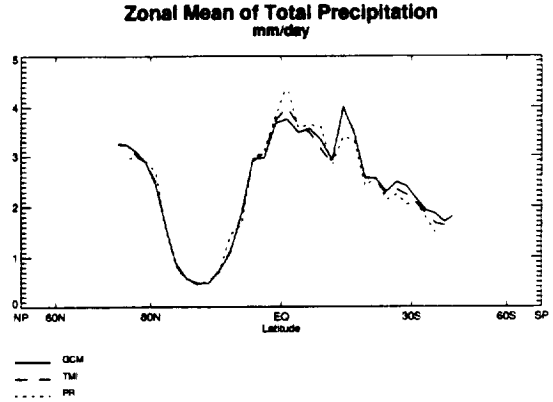
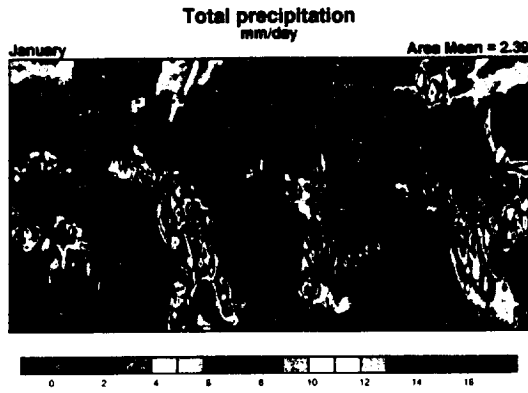


Figure 6

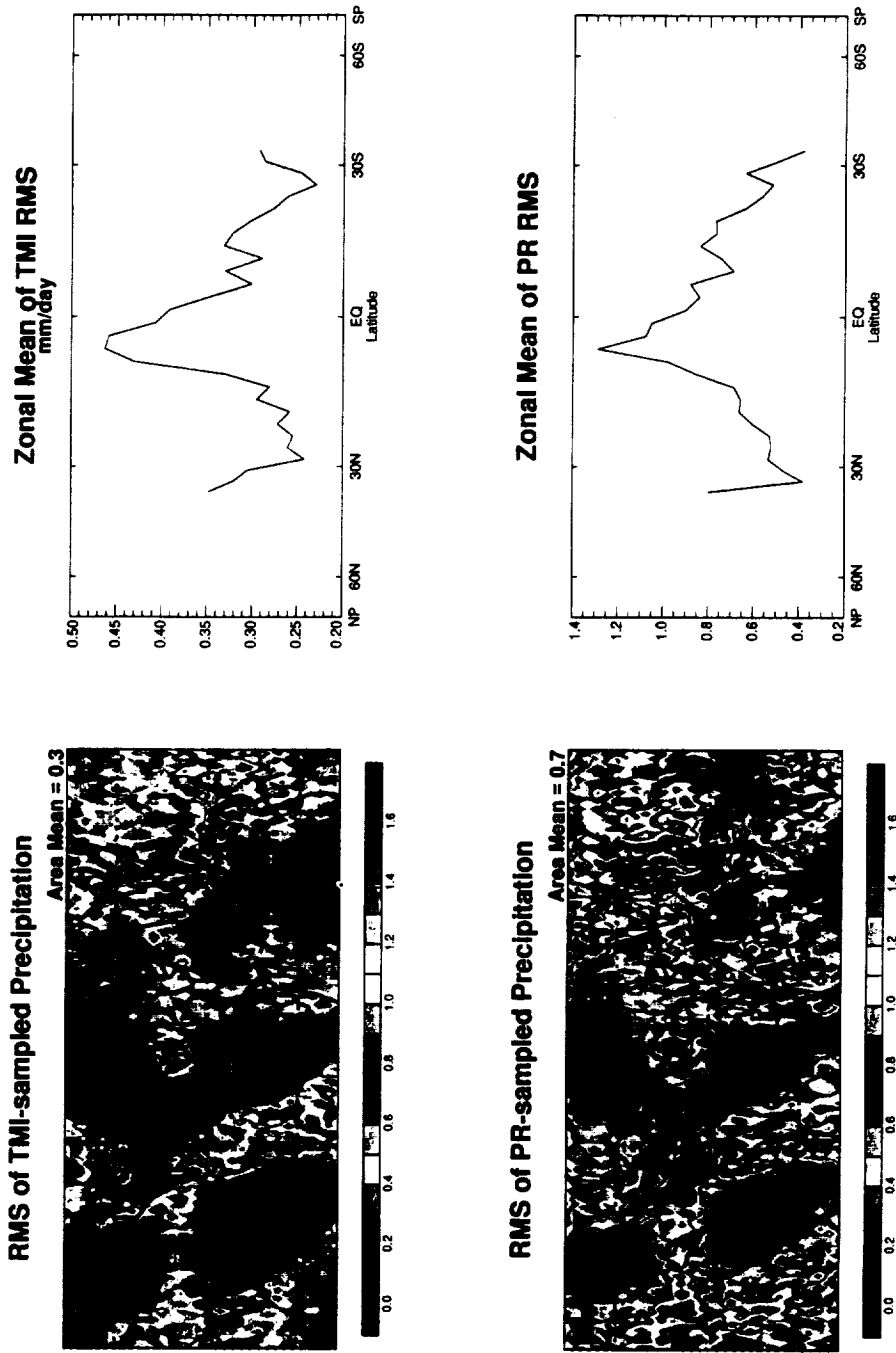


Figure 7

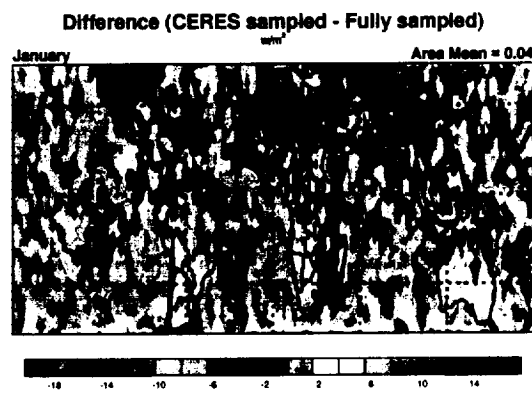
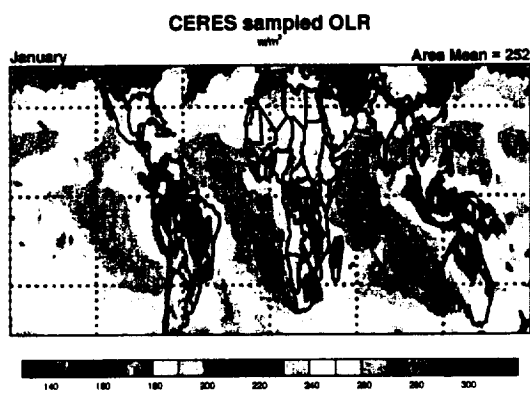
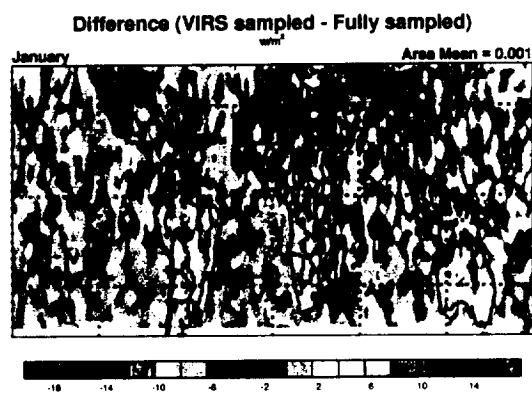
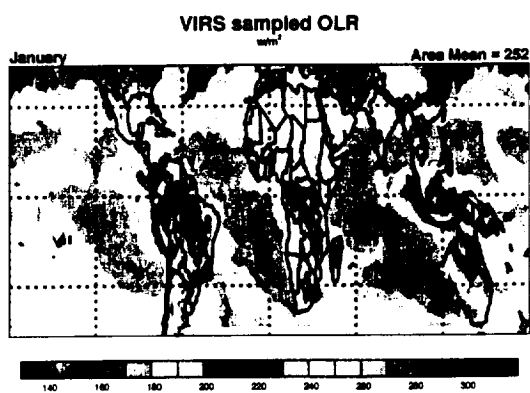
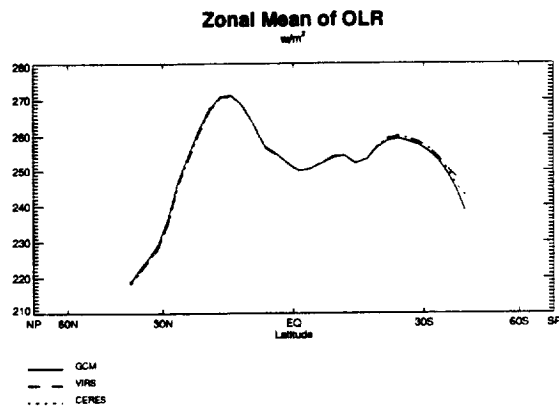
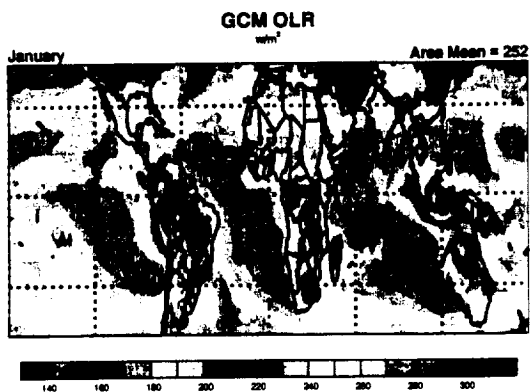


Figure 8

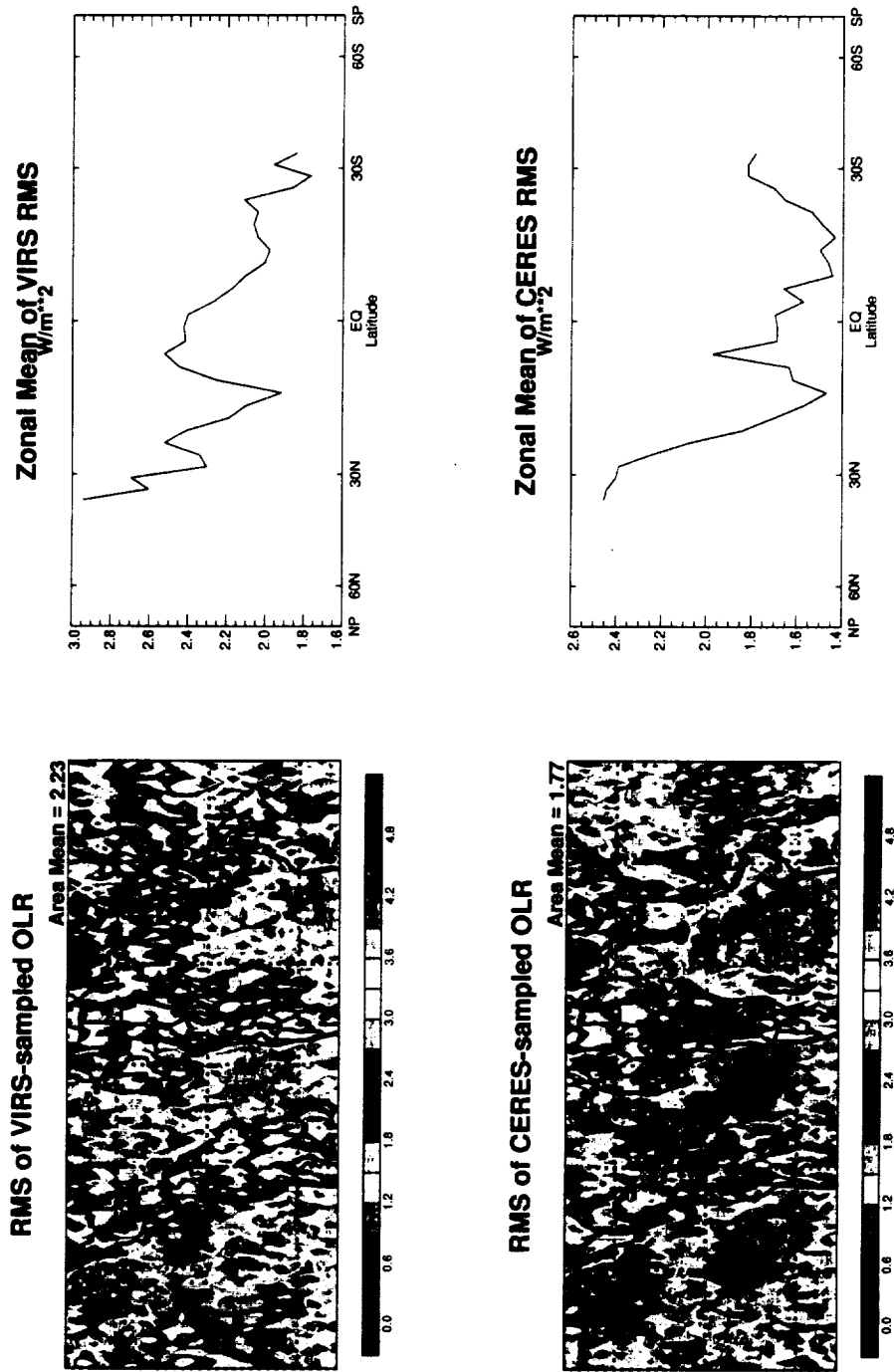


Figure 9

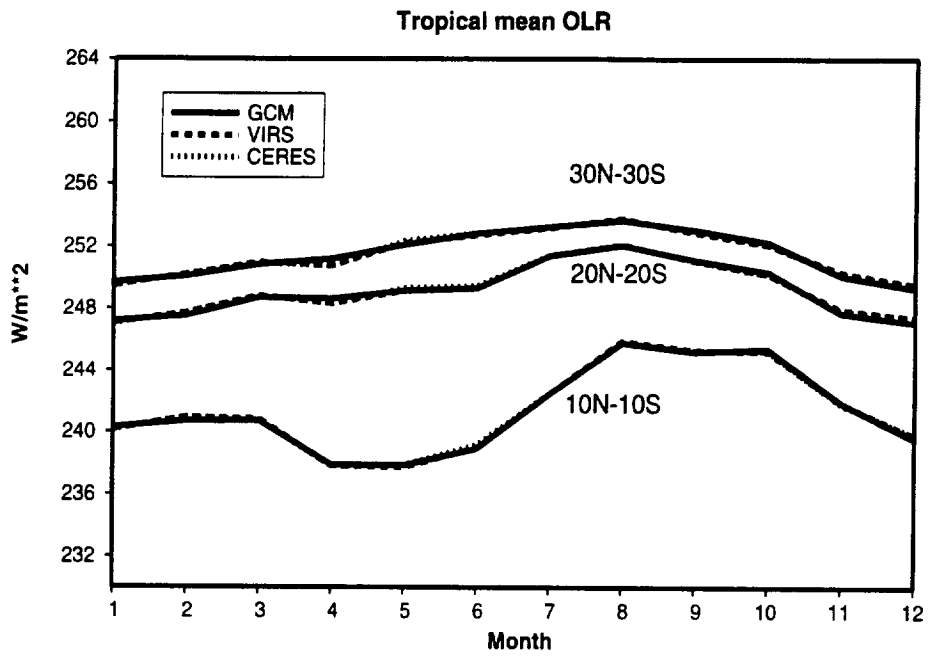
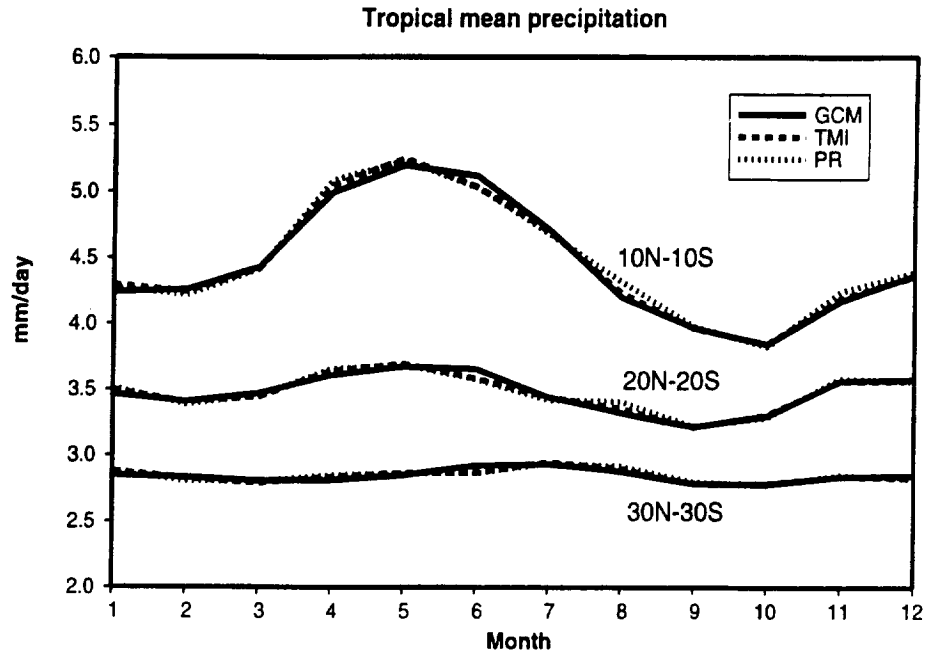


Figure 10a

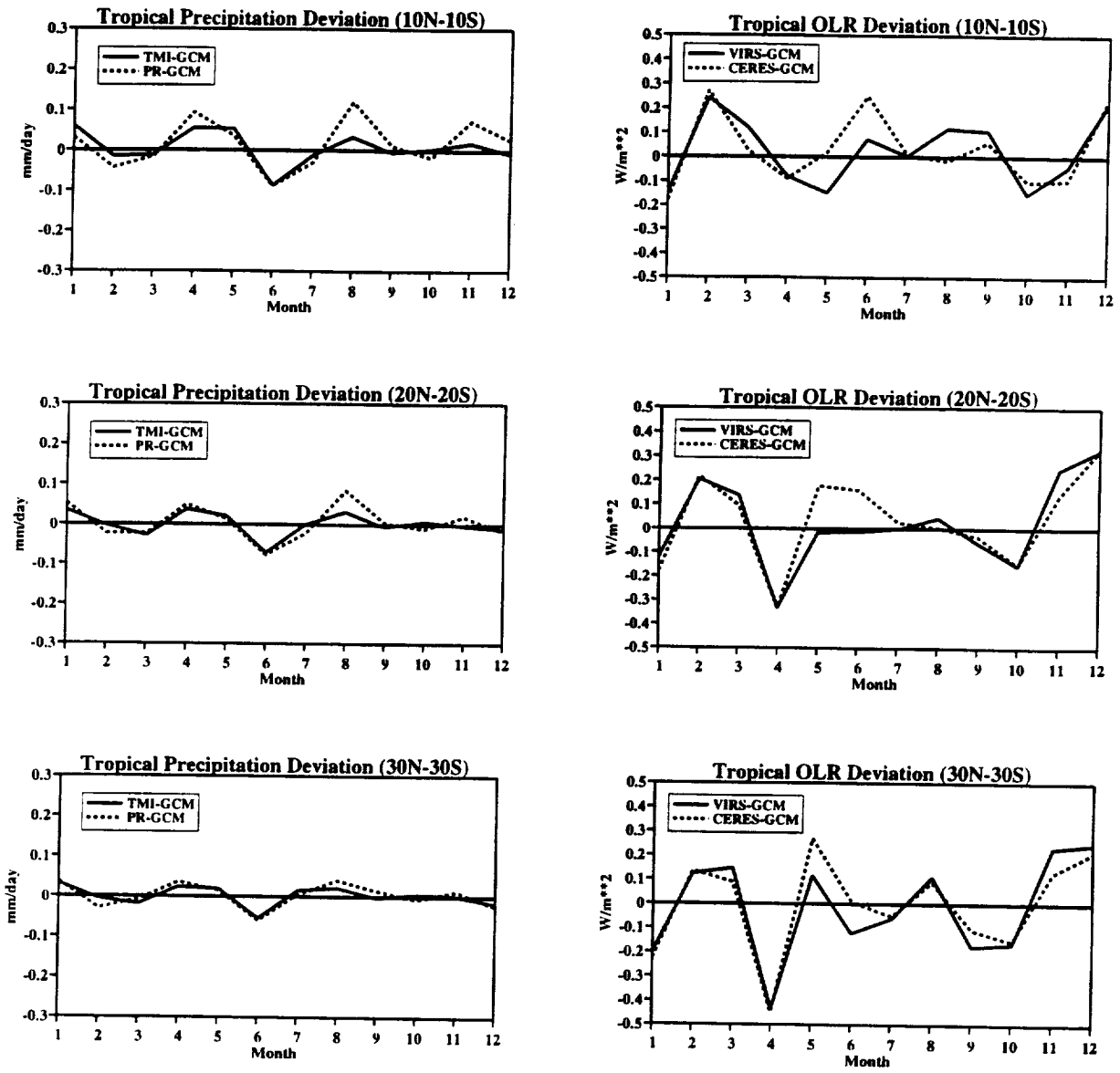


Figure 10b

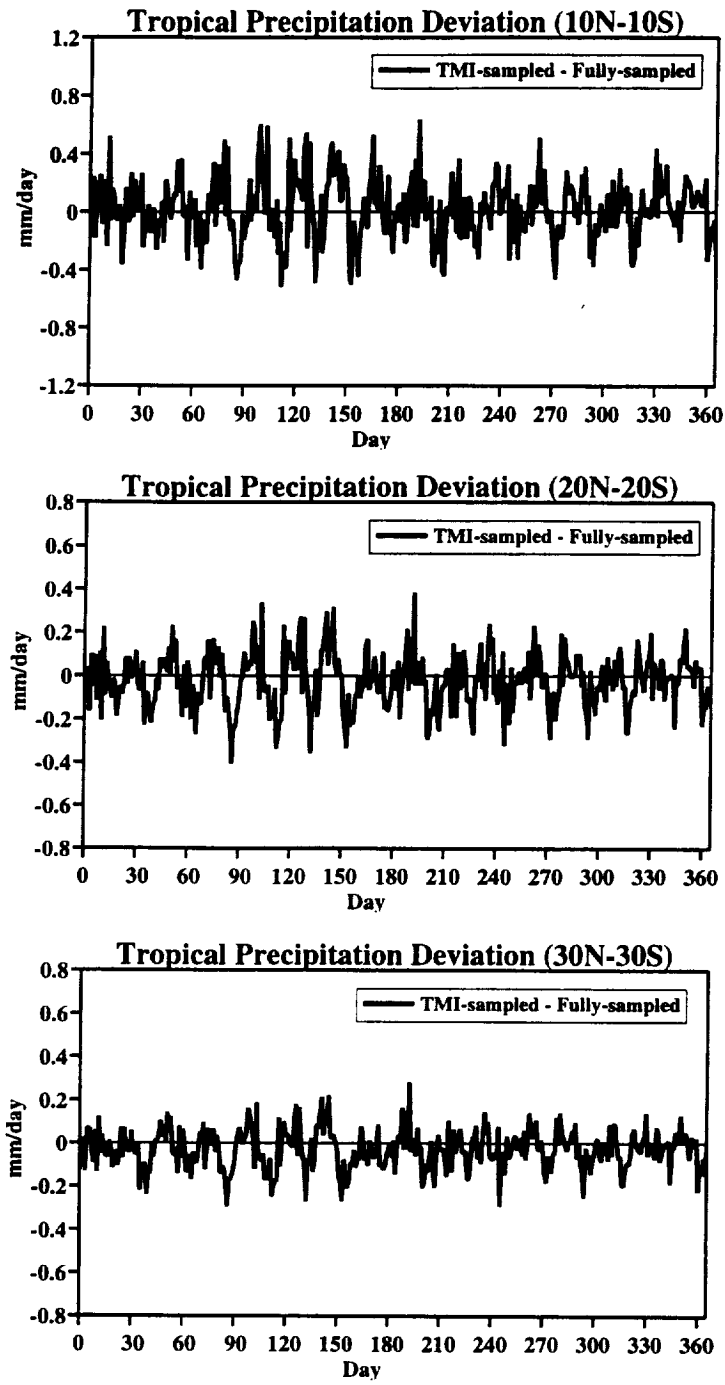
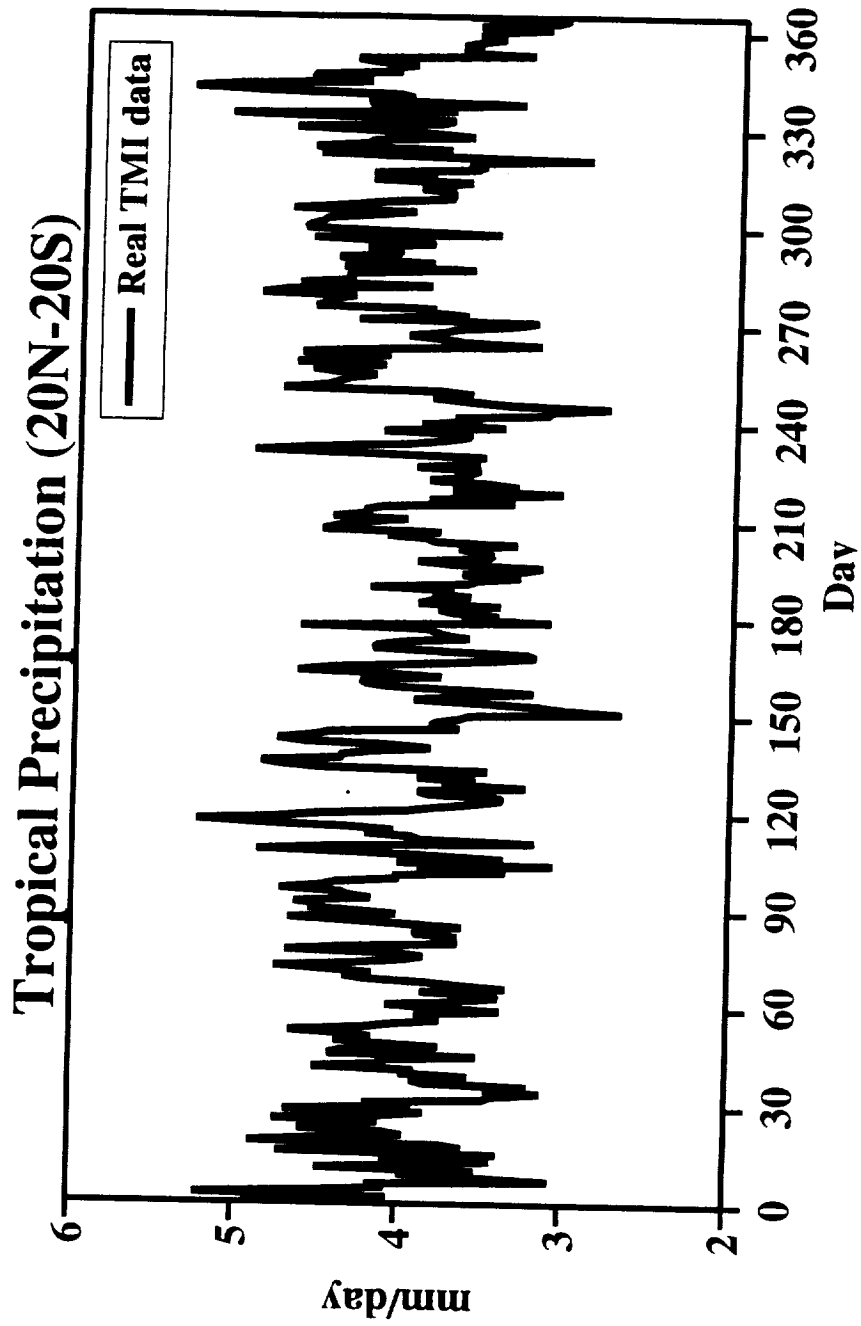


Figure 11a



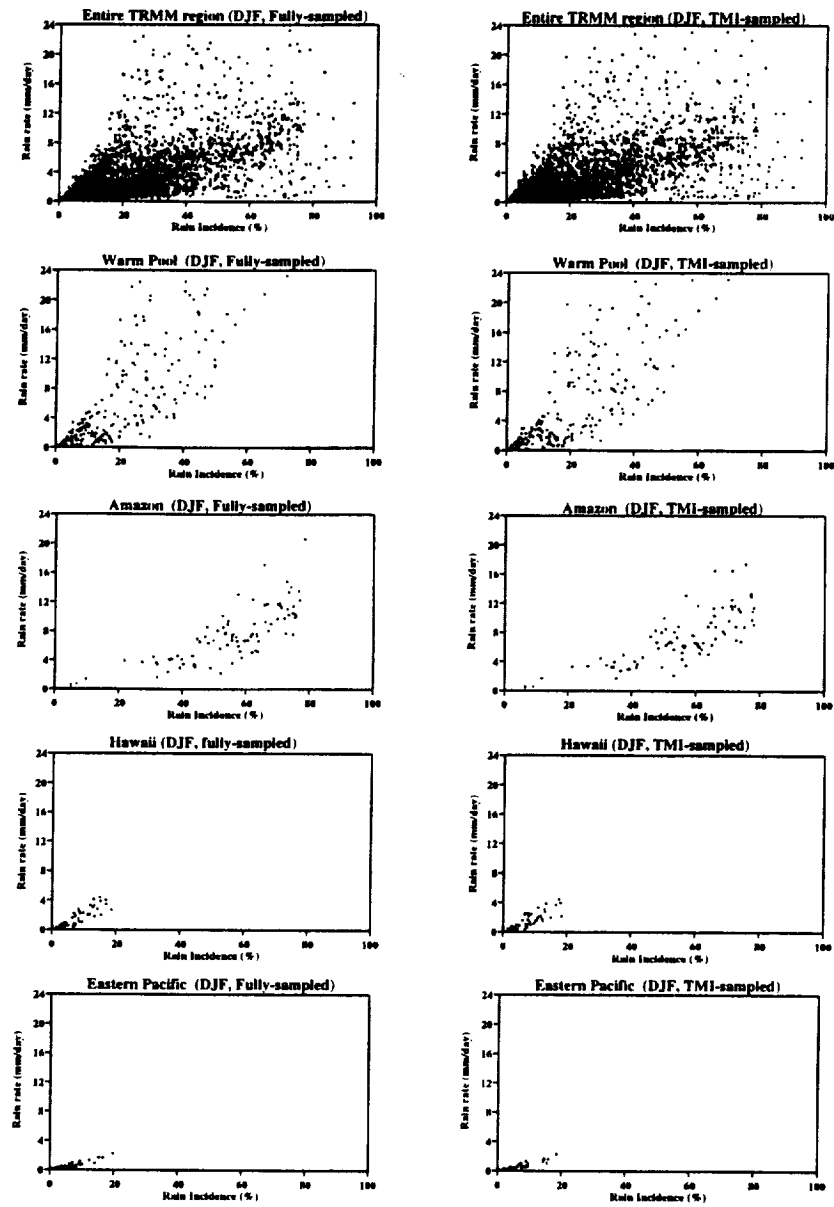


Figure 12

Figure 11b

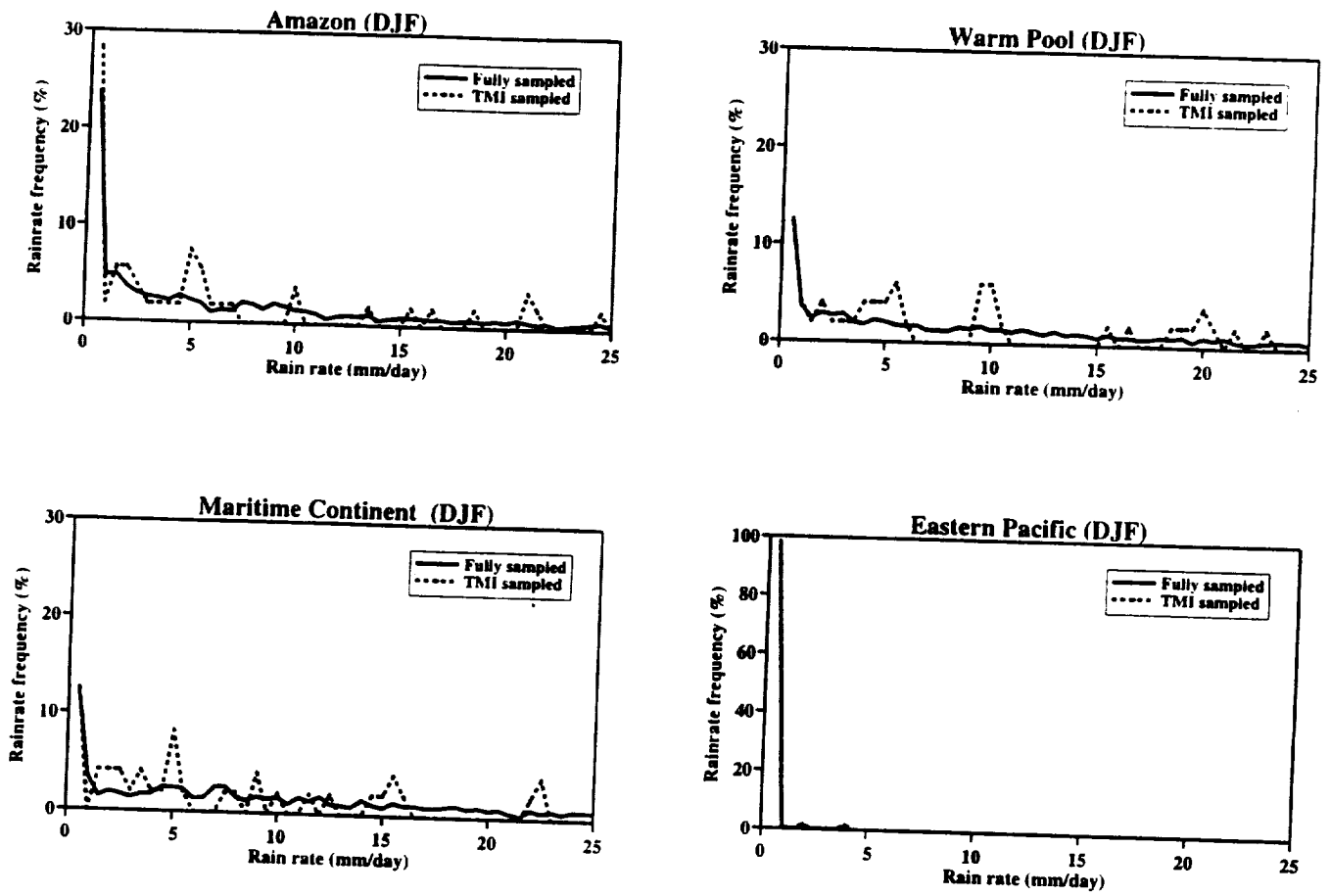


Figure 13

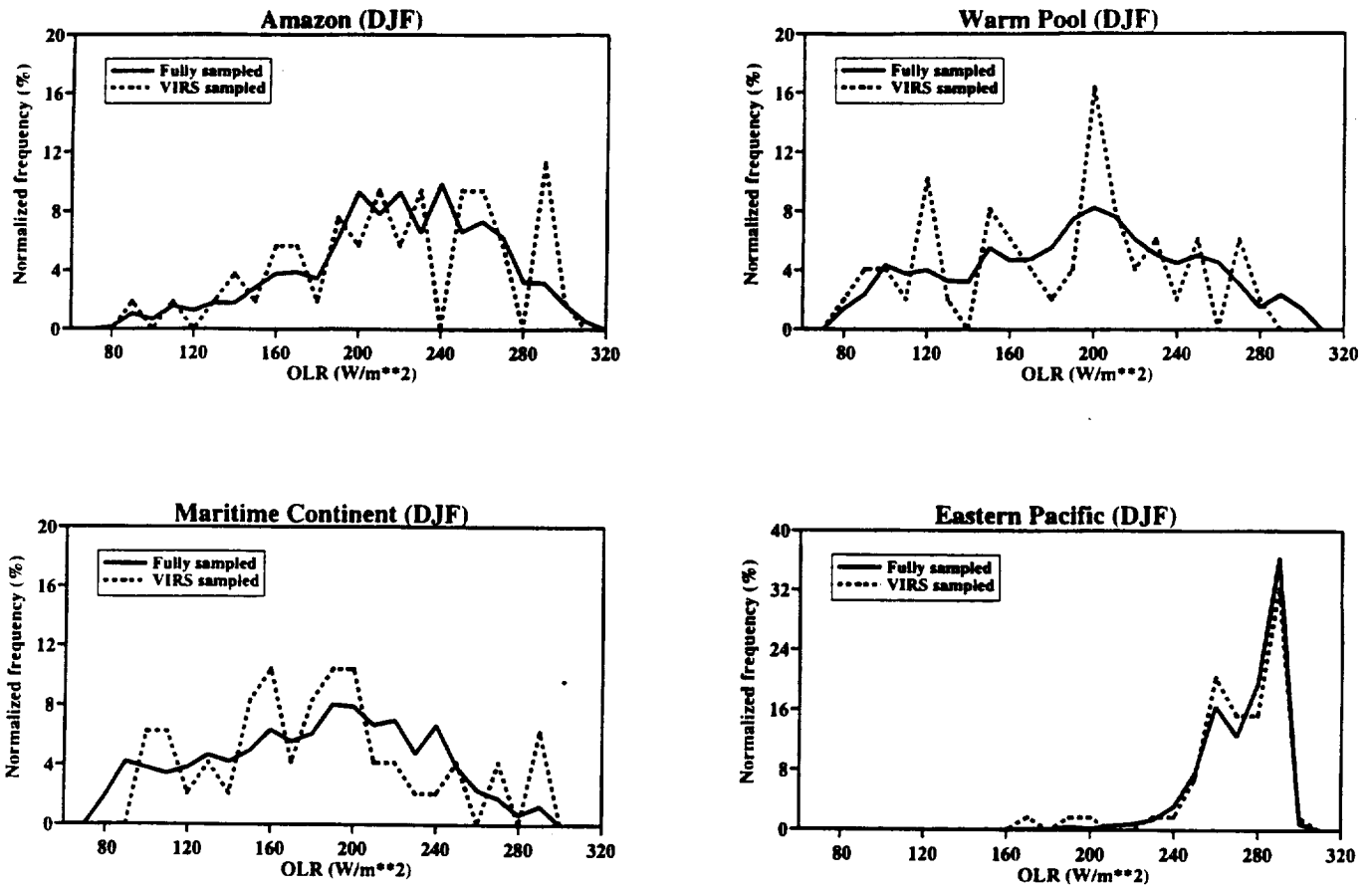


Figure 14

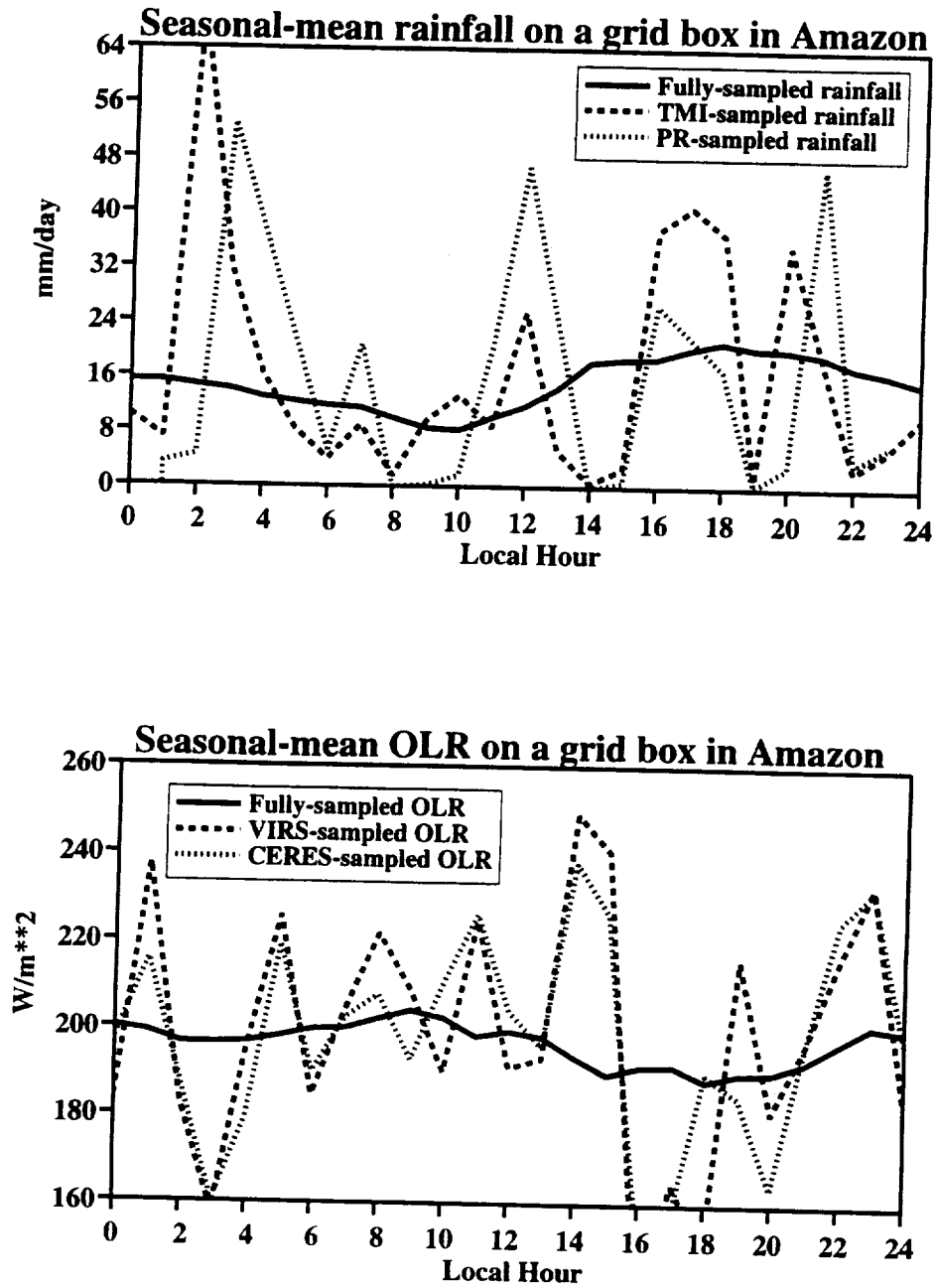


Figure 15

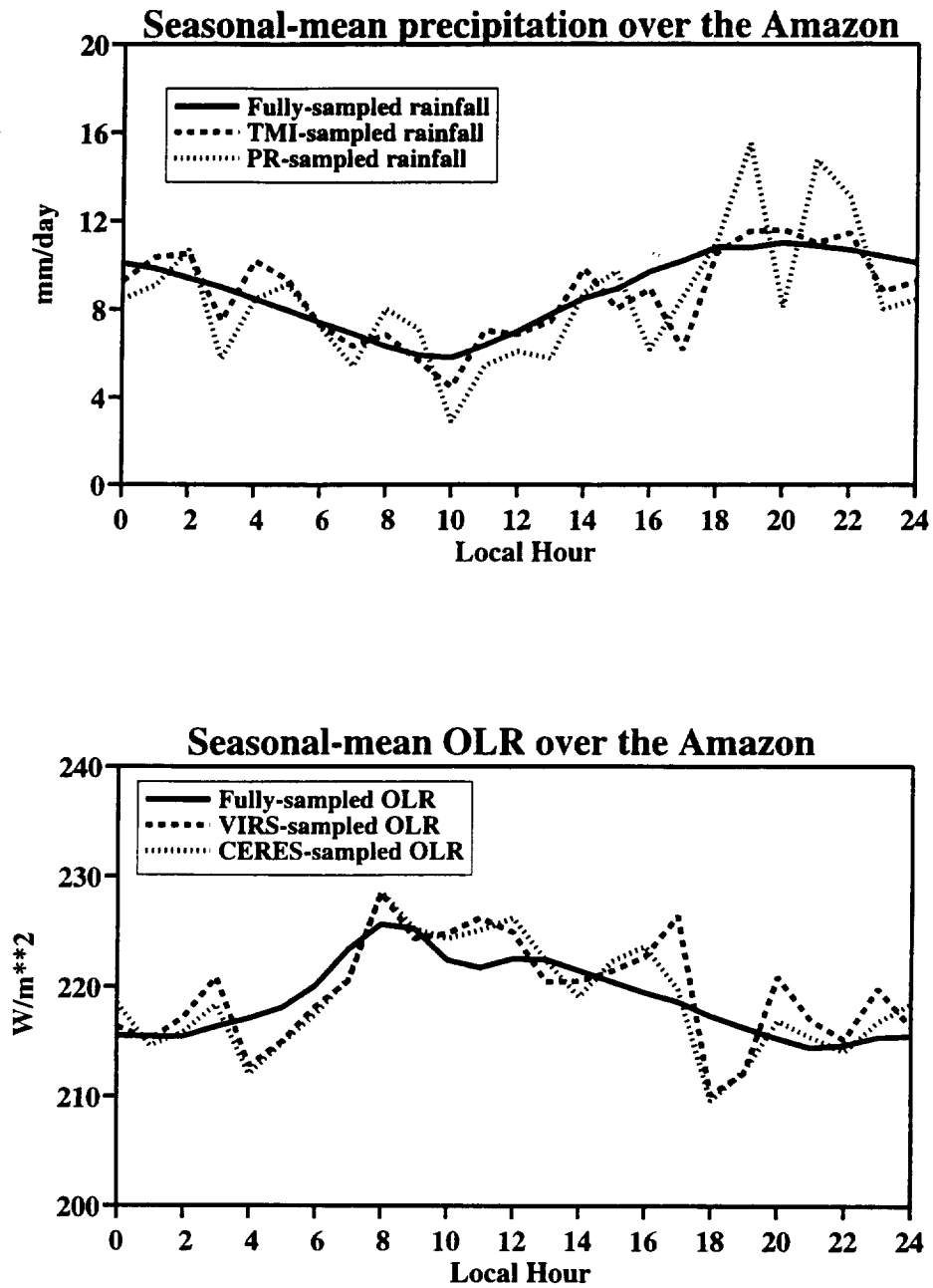


Figure 16

	Swath width (km)	Sensor type	Observed channels	Main products
TMI	760	passive microwave	5	rainfall, hydrometer profiles
PR	220	positive microwave	2	rainfall, storm struc- ture
VIRS	720	visible and infrared	5, narrow bands	brightness temperature
CERES	2000	visible and infrared	broad band	radiative fluxes

Table 1: Characteristics of sensors aboarding the TRMM satellite.